Space and Time Modulations of Light with Metasurfaces: Recent Progress and Future Prospects

Elena Mikheeva, Christina Kyrou, Fouad Bentata, Samira Khadir, Sébastien Cueff, Patrice Genevet

HAL Id: hal-03798836
https://hal.science/hal-03798836

Submitted on 8 Oct 2022

Space & Time modulation of light with metasurfaces: recent progress and future prospects

Elena Mikheeva,[†,‡] Christina Kyrou,[†,‡] Fouad Bentata,[†,¶,§,‡] Samira Khadir,[†] Sébastien Cueff,[¶] and Patrice Genevet[*,†]

†*Université Côte d'Azur, CNRS, CRHEA, Rue Bernard Gregory, Sophia Antipolis 06560 Valbonne, France*

‡*These authors contributed equally*

¶*Université de Lyon, Institut des Nanotechnologies de Lyon–INL, CNRS UMR 5270 Ecole Centrale de Lyon, Ecully, 69134 France*

§*STMicroelectronics, 850 Rue Jean Monnet, 38920 Crolles*

E-mail: pg@crhea.cnrs.fr

Abstract

In this perspective , we discuss the different opportunities offered by time-modulated metasurfaces for dynamic wavefront engineering and space-time photonics. Efforts in co-designing a photonic response while taking into careful consideration the switching/tuning mechanisms - including thermal, electronic, optical, chemical, and/or mechanical actuation - are essential for achieving sufficient amplitude, phase, and/or polarization modulation. Here, we examine in detail how the key enabling photonic technologies -currently available and relying on similar tuning mechanisms- can be applied for the conception of tunable metasurfaces. We review the latest developments

and discuss the advantages and limitations of each approach, providing the reader with a clear vision of the current state of the art in active metasurfaces. We also address the readiness of each technological approach to drawing short and long-term application perspectives. Finally, we discuss perspectives for spatiotemporal metasurface modulation opening new horizons towards unlimited wavefront engineering capabilities.

Keywords: tunable metasurfaces, reconfigurable metasurfaces, Space-Time modulation

Introduction

Optical metasurfaces are ultra-thin components made of sub-wavelength arrangement of optical resonators, or nanopillars, designed with spatially varying structural properties (for more details see review papers in references[1–3]). The variation of the geometry or material properties of these nanoscale elements, often called optical building blocks, introduce spatial variation on the reflected and transmitted electromagnetic fields. As a consequence, the reflected, and/or transmitted, light properties are modified. Various impressive results have been published over the last years, demonstrating phase, amplitude and polarization encoding.[4–16] So far, we can classify the existing optical mechanisms of interest to achieve light modulation as follows: 1) the utilization of resonant scattering,[17] 2) the phase accumulation during light propagation in truncated waveguides[18] where the transmitted phase ($\phi = 2\pi n_{eff} h/\lambda$, n_{eff} and h represent respectively the effective index of the fundamental mode and the nanostructure height) is imparted by the mode of the nanostructure only, 3) the orientation-dependent phase retardation, also called Pancharatnam-Berry (PB) phase[19,20] and 4) the recently proposed topological phase obtained by encircling optical singularities.[21] Resonant scattering designs can be also separated into local and non-local metasurfaces depending on the nature of resonances excited in the structure (not to mix up with local and global external stimuli application). While local metasurfaces leverage the response of a single meta-unit (such as multipolar resonances or localized surface plasmons), non-local

2

metasurfaces support collective modes in a periodic structure such as guided-mode resonance in a substrate, surface lattice resonance, or quasi-bound states in the continuum. Non-local metasurfaces allow for the spectral tuning of a narrow band surface response, which might thus be advantageous for various applications.[22–25]

In a general case, metasurface building blocks are inherently passive, fabricated once and for all to perform a fixed optical functionality. While passive metasurfaces have extremely interesting applications perspectives, in particular by considering their integration in optical and optoelectronic systems,[26–29] the optical responses of the components are not flexible. Efforts in achieving light modulation with ultra-thin metasurfaces would open serious research opportunities and unlimited industrial applications. The purpose of this perspective article is to summarize which are the enabling technologies that can be reasonably considered for achieving reconfigurable metasurfaces. Reconfigurable (also called active) metasurfaces have been realized long ago at microwave frequencies using active elements such as PIN-diodes or varactors, as discussed in various articles.[30–37] However, as the wavelength scales down, this option is no longer available and tunability has to be introduced by changing either the properties of materials composing the metasurface building blocks or the optical properties of the surrounding medium using external stimuli. Several manuscripts have been published to categorize tunable metasurfaces, for example, by grouping them according to the tuning mechanism: electrical, mechanical, optical, thermal,[38] and chemical tuning.[39] It is possible to differentiate them according to the types of materials, such as transparent conductive oxides, ferroelectric materials, 2D materials (graphene, MoS_2), phase-change materials, liquid crystals, and semiconductors.[40] Other reviews have distinguished electro-mechanical switching,[41] and free-carrier density modulation[42] into separate categories. In addition to thoroughly discussing different tuning mechanisms, one of the previous reviews also provides an insight into applications of dynamic metasurfaces, in particular, focusing on the Spatio-temporal devices.[43] Another reported review divides tunable metasurfaces into hybridized ones (e.g., combining active medium with metals) and metasurfaces with building

blocks made of active material.[44] Here, we propose to draw prospects of this research field by analyzing how the existing technologies help improve the level of development of tunable metasurfaces and how they help bridge the gap between academic research and industrial applications.

Figure 1 summarizes schematically the content of this perspective article. It shows a programmable metasurface featuring arbitrary electromagnetic response in space and time activated using different tuning mechanisms. On the right panel of Figure 1, we show a selection of perspective tuning mechanisms including phase change materials, electro-optic effect, chemical reactions, mechanical tuning, and liquid crystal reorientation. Their advantages and bottlenecks, and their potential for large-scale industrialization are discussed in the first part of the article. The success in the implementation and integration of these devices in complex systems rely on their compatibility with well-established, low-cost, and scalable manufacturing process. Voltage addressing using electronic elements and driving integrated circuits (ICs) has been selected as probably one of the most, if not the most, promising routes for active metasurfaces. Figure 1 illustrates schematically a time-varying metasurface based on different tuning mechanisms and its possible applications. Time-varying functionality is achieved by applying an external stimuli such as electrical bias. Electronic devices providing real-time digital modulated voltages outputs, such as field-programmable gate array (FPGA), can switch the states of the meta-units. Real-time programming of the meta-surface requires, for instance, a micro-controller unit (MCU) equipped with an advanced driving algorithm to regulate the FPGA outputs. This device aligns very well with the current quest in the industry for achieving a high degree of automation in decision-making. Internet-of-Things (IoT) and Autonomy-of-Things (AoT) are driving the high demand in systems offering high-end synchronization and intercommunication, and we believe that active metasurfaces could certainly offer interesting applications perspectives in these areas. These applications include LiDAR (Light imaging Detection and Ranging) sensors for advanced assisted driving systems (ADAS) or even full autonomous driving,[45] wearable devices

4

for AR/VR applications,[25] robotic industry 4.0,[46] microscopy and image treatment,[22] etc. We finally provide insights on academic and relatively unexplored research topics dealing with spatiotemporal metasurfaces. We illustrate a non-reciprocal metasurface that can be realized in case of ultra-fast time modulation, i.e. a device in which time-reversal symmetry is broken and that enables asymmetric trajectories accompanied with frequency shifting. We show an example of non-reciprocity together with others to illustrate the versatility and diversity of applications of tunable metasurfaces.

From current Key enabling technologies to tunable meta-surfaces

From Phase-Change Memories to active Metasurfaces

Phase-change materials (PCMs) for photonics have been a booming field of research for roughly a decade.[47] The tantalizing potential of PCMs for dynamic metasurfaces can immediately be understood by summarizing their most salient features : (i) large refractive index modulation (one of the largest compared to other considered tuning mechanisms, $\Delta n \geq 1$ as shown in Table 1), (ii) fast, reversible – and for some of them non-volatile – switching, (iii) multi-stimuli switching (thermal, optical, electrical...), (iv) potential monolithic integration at the nanoscale.

The large body of research on PCMs for photonics is described in a few reviews that can be found in the literature (see e.g.[47–50]), some of which are entirely dedicated to PCM for metasurfaces.[51,52] Most of these reviews are focused on 'standard' PCMs such as chalcogenide PCMs (GeSbTe or GeTe) or phase-transition oxides such as VO_2. Very recently, a new category of PCMs – which we hereby call 'low-loss PCMs' – has emerged, comprising three main materials: Sb_2S_3, Sb_2Se_3 and GeSbSeTe. Given the advantageous properties of these emerging materials, they have the potential to outclass standard PCMs. After reviewing
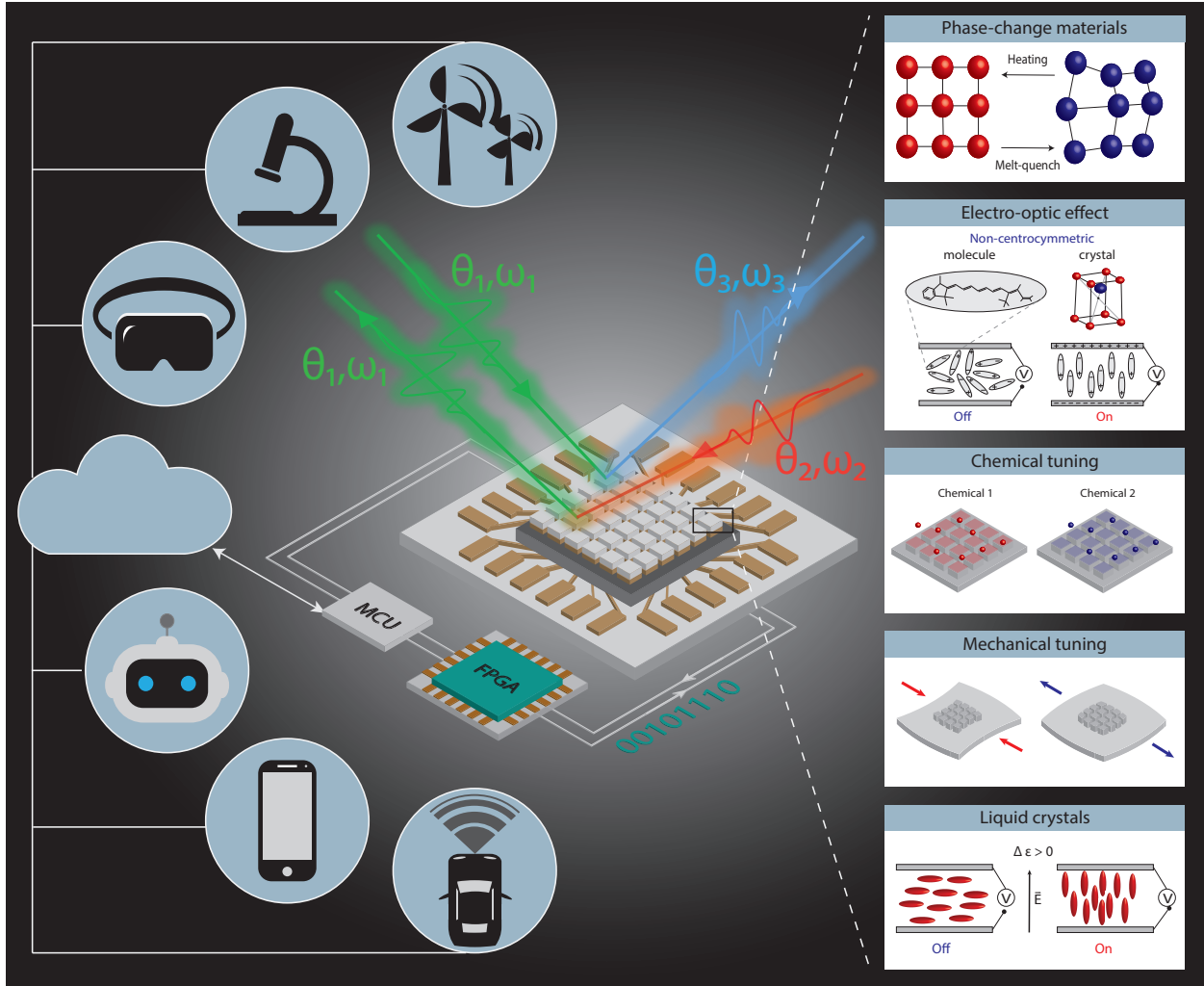
Figure 1: Schematic figure representing a dynamic metasurface that addresses space &/or time modulation. Several modulation mechanisms including phase-change materials, electro-optic effect, chemical tuning, mechanical tuning, and liquid crystals are illustrated on the right panel. Digital controllers and operation software dedicated to the complex metasurface architecture have to be considered in the future according to the applications of interest (left panel). Illustration of the optical effects obtained by breaking the reciprocity including non-reciprocal refraction and frequency modulation at interfaces (appears at high time modulation speed only).

very recent results obtained on standard PCMs, we, therefore, dedicate a large part of this subsection to recent works exploiting the low-loss PCMs for metasurfaces.

Standard PCMs:

PCMs are unique materials whose physical properties depend on their crystallographic states. Two classes of materials are usually referred to as PCMs: chalcogenide PCMs (e.g.

6

Table 1: Key metrics for different PCMs: complex refractive index at two wavelengths 630 nm and 1550 nm (from left to right: minimum real part of refractive index, contrast $\triangle n$ between crystalline and amorphous state, extinction coefficient at crystalline state), switching temperature, energy density (the switching energy per unit PCM volume) and switching speed. The energy densities and switching speeds were found to strongly depend on design, switching mechanism (optical or electrical) as well as on the preparation methods and deposition conditions

PCM	n_{min} , $\triangle n$, k_c		T_c	Switch. Energy	Switch. Speed
	$\lambda = 630nm$	$\lambda = 1550nm$			
GST	3.63, 0.52, 3.72	3.63, 2.1, 1.8	180 °C	$1.3 \times 10^{-2} fJ/nm^3$	50 ns
VO_2	2.56, 0.1, 0.3	1.36, 1.4, 2.9	70 °C	$1.5 \times 10^{-9} fJ/nm^3$	$\sim$ ns- μs
GSST	3.7, 1.9, 2	3.21, 1.8, 0.3	400 °C	$2.2 \times 10^{-2} fJ/nm^3$	100 ms
Sb_2S_3	3.11, 0.89, 0.58	2.69, 0.54, 0	280 °C	$5.9 \times 10^{-2} fJ/nm^3$	75 ns
Sb_2Se_3	4.4, 1.17, 1.27	3.7, 0.7, 0	200 °C	$7.9 \times 10^{-2} fJ/nm^3$	100 ms

Ref.[53–56] The values reported here should therefore not be seen as fundamental ones but rather as state-of-the-art metrics that we collected from different works[56–62] which we find representative of the different values reported in the literature.

GeSbTe) and phase-transition oxides (e.g. VO_2). These two categories share similarities in that a modification of their structural atomic arrangements produces large modulations of their complex refractive indices (Table 1). However, the underlying physics behind their respective modulations is different (for this reason, some researchers consider that they should not be grouped under the same label of PCM). We briefly describe below the basic physical principles that produce such drastic physical modulations.

VO_2 presents a first-order transition from a monoclinic insulating state at room temperature to a tetragonal metallic state at temperatures above 70°C. This material is a famous example of Mott insulators: according to band theory, it should be a metal but behaves as an insulator. The physical reason behind this phenomenon is strong electron correlations between free carriers that prevent electrical conduction.[50,63] A moderate input of energy on that system can break the equilibrium and trigger a transition from an insulating state to a conductive state. This so-called insulator-to-metal transition happens in a very short time (down to the femtosecond timescale).[64–66] Conversely, the metallic state is volatile, and hence switching back from metallic to insulating is typically slower, as it requires evacuating the excess energy/heat brought by the first excitation. Note that the on-off switching cycle

is accompanied by a hysteretic behavior that can prove useful for some applications.

VO_2 is widely used for its tunable plasmonic resonance in the metallic state that switches off in the insulating state in the IR.[67–69] Recent papers show that nanostructures made of- or combined with-VO_2 exhibit Mie resonances in both insulating and metallic states, opening the door for new metasurface designs such as tunable Huygens Metasurfaces in both the visible and near-infrared range.[70–72] As mentioned previously, the transition can also be controlled by electrical means. Based on that principle, spectral modulation[73] and optical phase modulation[74] were recently demonstrated using electrically-driven VO_2-based metasurfaces operating around the telecom wavelength range. Apart from all the mentioned designs, thermally-tunable VO_2-based absorbers were also successfully implemented.[75,76] Additionally, the metastable metallic state, even though volatile, can be used at advantage to optically or electrically write devices with large flexibility and easiness to erase. This phenomenon was used to demonstrate an optically rewritable photonic 'metacanvas' in which the hysteresis was used as a means to hold the metallic patterns by maintaining the sample at a moderate temperature (70°C).[77] Using this method, arbitrary patterns for diverse optical responses can be written and erased very easily. Given the lower optical absorption of insulating VO_2 in the mid-infrared and THz ranges, several recent works reported efficient electrically-controlled multifunctional amplitude switching VO_2-based metasurfaces in these wavelength ranges.[78,79]

The other class of PCMs - chalcogenide-based PCMs - possess properties typical of a semiconductor when it is amorphous: a moderate refractive index and a dielectric nature. However, when the same material is crystallized, its refractive index becomes very large and the material becomes conductive. Such behavior is very much unlike conventional materials (e.g. amorphous and crystalline silicon) and is due to an unconventional bonding mechanism in the crystalline state, recently coined 'metavalent bonding'.[80,81] Chalcogenide PCMs can be composed using alloys of Germanium (Ge), Antimony (Sb), Tellurium (Te), Selenide (Se), and Sulfur (S). This creates a library from which materials can be selected based on

the bandgap, complex refractive index, and required properties.[40] Among them, germanium-antimony-telluride ($Ge_x Sb_y Te_z$ with various stoichiometry) is one of the most studied PCMs for photonics. It has high cyclability (10^{15}), high switching speed, high retention (~ 10 years) and low power consumption depending on the unit cell size.[51,82,83]

Provided the switching of Chalcogenide PCMs physical properties is governed by their crystallization, such modulation is by definition non-volatile. It is also reversible through a re-amorphization process that is usually obtained by a melt-quenching method, in which a PCM is heated above its fusion point and subsequently cooled down at rates faster than the crystallization kinetics (more than $10^9 Ks^{-1}$ for GST).[47,84] Re-amorphization is an extremely fast process that can be triggered by a single-pulse femtosecond laser or nanosecond electrical pulse. The overall cycling time is limited by the crystallization process which is slower than the amorphization.

There are several ways to switch these materials between states, such as thermal annealing[84,85] or optical writing with pulsed lasers.[86,87] However, one of the most important mechanisms is electrical switching as it promises future integration with other microelectronic technologies. This kind of switching is well-developed for phase-change random-access memory (PC-RAM) technology that has a data transfer rate greater than gigahertz (having $\sim 10nm$ cells).[88,89] However, scaling it up to $\sim 100nm$ and larger sizes becomes challenging due to non-uniform phase transition within a bulk of PCM, especially for a cooling process. This problem has been addressed with electro-thermal switching of metasurfaces, which opened a route to co-designed photonic and electronic devices.[56,90–92]

In particular, electro-thermal switching leveraging an integrated micro-heater layer provide an efficient means to locally tune PCMs. Wang et al. recently demonstrated a GST-based metasurface placed on top of a thin silver film (Figure 2a) that plays both the role of a plasmonic antenna and a micro-heater that uniformly heats the structure (unlike direct current injection with filament in PC-RAM).[90] Both crystallization and amorphization are carried out by running current pulses: lower current pulse with longer duration crystallizes

9

the PCM, while shorter and higher current pulse leads to re-amorphization. The metasurface acts as a perfect absorber when GST is crystalline (due to destructive fields interference) and starts reflecting light when it is amorphous. Experimental results show reflection switching from $\approx 4.3\%$ to $\approx 14.5\%$ at 700 nm wavelength, as shown in Figure 2b. The authors report a 10 kHz modulation speed, for this hybrid PCM metasurface (Figure 2c). Abdollahramezani et al. also recently demonstrated electrical switching of hybrid GST-Au metasurface supporting two distinct plasmonic modes that can be tuned by the GST layer, hence modulating the reflection amplitude in the NIR. The device exploits a tungsten micro-heater enabling an electrical control of the crystallization state of the GST layer.[93]

An alternative recent strategy for phase transition is the solid-liquid phase transition. Bismuth-nanostructures are nanoparticles based on Bismuth monoelement used because of its solid-liquid optical contrast with low melting points of about 270°C. Recently, Alvarez-Algeria et al.[94] demonstrated the relevant properties of a random distribution of Bi-nanostructures in a dielectric matrix (PCRMs Phase Change Random Metasurfaces). A nanosecond pulsed laser was used to melt the Bi-nanostructures with different filling factors allowing a high optical contrast between the solid and liquid states (On/Off state) and fast switching up to 10 ns and semi-volatile behavior which means staying at the melting phase without permanent power supply for a given time duration. This was enabled by using latent heat to maintain the temperature at phase transition and by designing the distance between the Bi-nanostructures and the Si substrate which also plays a heating role which lengthens the melting time and thus the melting phase $> 1\mu s$ (On-state), and high cyclability up to 100 000 cycles without damaging the sample.

Emerging low-loss PCMs:

The standard PCMs such as GST and VO_2 present a high optical absorption in the visible and NIR spectral range which limits their utilization in realistic optical systems. Recently, alternative low-loss materials with high contrast in refractive index and low extinction coefficient in the visible and NIR regime have emerged.[60–62,95,96] For example, Sb_2S_3 presents

a transparency window from 610 nm to the NIR with a relatively large index contrast and cyclability higher than 1000 cycles,[60] and Sb_2S_3 has a transparency window from 800 nm to the NIR, a larger index contrast and relatively high cyclability (4000 cycles).

High refractive index and transparency make Sb_2S_3 and Sb_2Se_3 good candidates for electronic displays or metascreens.[96] Recent works report such meta-displays designed using anisotropic pillars supporting multipolar resonances, as shown in Figure 2d. A single metascreen can generate two colors for two different polarization of visible light that can be switched when PCM changes between its amorphous and crystalline states. Figure 2e. shows two different images for two perpendicular linear polarization for the amorphous phase. Switching these parameters changes the display colors and, with the right optimization, makes a part of the image disappear.

As in the case of GST discussed previously, designing the heating element for low-loss PCMs is an important step to provide a uniform heat flow to the meta-atoms, in order to increase the switching capabilities (e.g., reversibility) and to optimize the power supply without compromising the optical efficiency. For example, Zhang et al[56] used a gold thin film that acts both as a heater and an optical reflector for their GSST-based metasurface. The design of the micro-heater includes a curved shape and a larger surface area than the metasurface, allowing a directional current flow and a uniform heat distribution to the meta-atoms. Interestingly, the slower crystallization kinetics of GSST compared to GST enables optimizing the heat distrtibution, reducing the power loss around the telecommunication wavelength (about $1.5\mu m$) and using a larger thickness of PCMs (about 250 nm).

These very promising recent results combine both low-loss PCMs with electrical control of their crystallization state. So far, the architecture of these first demonstrations can only enable the switching of devices as a whole. Said otherwise, they cannot provide direct control over each individual meta-atoms. Such an individual control of elements was recently demonstrated by optical means using an external laser to switch separate PCM-based meta-atoms.[97] While there are no fundamental limitations to a direct electrical control of individual PCM
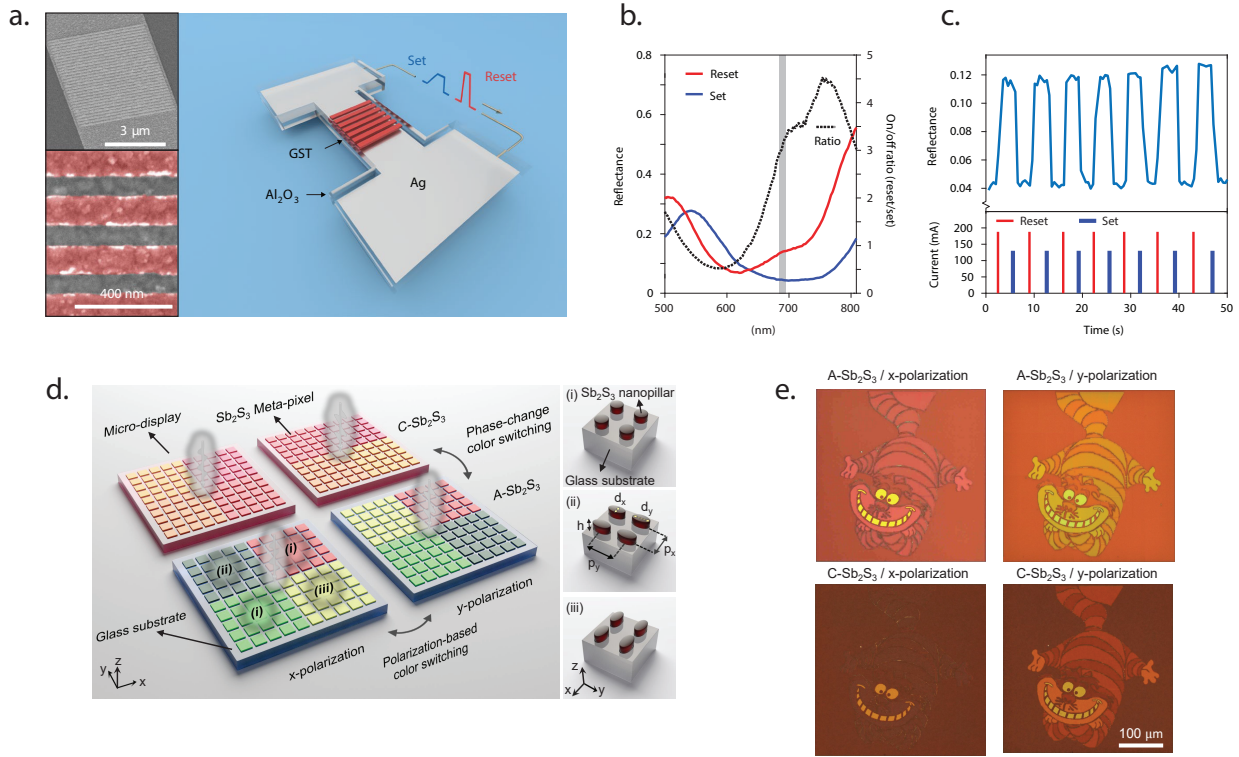
Figure 2: Highlights: metasurfaces based on phase-change materials a. Tunable GST meta-surface placed on optically thick silver stage which is heated by set and reset current pulses. This leads to GST meta-atoms being switched between amorphous and crystalline states b. Experimental reflection spectra for metasurface from (a) being set and reset with current pulses. c. Demonstration of switching metasurface from (a) in time between reflecting and absorbing states corresponding to set and reset condition from (b). (a-c) Republished with permission of Springer Nature, from;[90] permission conveyed through CCC, Inc. d. Reflective color displays consisting of low-loss PCM Sb_2S_3 anisotropic particles arranged periodically and forming meta-pixels. Each meta-pixel produces different colors for 2 perpendicular linear polarization, both produced colors can be tuned by switching Sb_2S_3 pillars with an on-chip heater made of conductive transparent oxide. e. Images obtained by using the structure shown in (d) with meta-pixels in the amorphous and crystalline state for x- and y-polarization. (d,e) Reprinted with permission from.[96]

meta-atoms, the current technical bottleneck is common for all the tuning mechanisms: how to electrically connect and independently drive thousands of nano-elements? One plausible route is to revisit current phase-change random access memories (PC-RAM). Such PCMs as GST are compatible today with 300 mm industrialization and ST Microelectronics already demonstrated phase-change based RAM integrating millions of nano-heater-controlled PCM cells, each addressed via an independent transistor in 28nm FDSOI eNVM technology for automotive Micro-controller applications.[89,98] The typical dimension of a nano-heater cell is

12

around 50 nm, separated by around 100 nm, i.e. sub-wavelength dimensions in the visible. This ensures that pixel-by-pixel tuning using nano-heater is a promising approach for the realization of tunable metasurfaces at optical wavelengths.

Compacting electrical modulators to functional surfaces

Metasurfaces based on Electro-Optic effect

Up to date, one of the best performances in terms of switching speed and low material losses for conventional optoelectronic devices have been achieved with electro-optical modulators, making use of the electro-optic (EO) effect. Considering the EO effect at the nanoscale for tunable optical metasurfaces would allow to decreasing distance between the electrodes and lower the electrical power required to address the modulation. The EO effect includes Franz-Keldysh effect (shift of the semiconductor absorption edge), Stark effect (splitting and shifting of energy levels in a quantum system, could be linear and non-linear), Pockels, and Kerr effect (linear and non-linear birefringence induced by an electric field).[99]

In particular, the Pockels effect is currently used in many light-modulation applications. It is generally present in non-centrosymmetric materials (crystals, polymers, metal-oxide materials) and the degree of induced changes depends on the electro-optic tensor defined by the material's structural properties. In such a material, the electric field introduces linear refractive index shift along one of the crystallographic axes, while maintaining the same refractive index along orthogonal axes. The refractive index change depends on the applied voltage amplitude and polarity, getting oriented due to the superposition of different forces. The shift introduces phase retardation between different polarization components and achieves dynamic control of the light properties. As the induced refractive index change is generally very small, large phase or amplitude modulation using conventional optoelectronic devices requires propagating and thus modulating the transmitting phase along sufficient thickness.

The resonant feature of metasurfaces might open the route to reduce the size of electro-

optic crystals while providing sufficient phase and amplitude modulation. EO materials were used in combination with metals, serving as an embedding medium surrounding resonant plasmonic structure,[100] as a part of metal-insulator-metal structure,[101] or as a nanoparticles layer combined with plasmonic nanostructures.[102] This metasurface already modulates reflection amplitude in the range of about 15 % for a relatively low actuation voltage of about $4 \ V$ and at an extremely high modulation cut-off frequency of about $20 \ MHz$.

Several current attempts to apply Pockels effects focused on using EO materials as resonant units, including the recently demonstrated metasurface made of lithium niobate crystal cylindrical posts.[103] Nanostructuring the lithium niobate thin film leads to lower-order multipolar resonances (in particular, resonance dominated by the electric dipole mode). By placing this structured surface between the electrodes (Figure 3a) and applying AC driving signal, the resonance position is shifted leading to a significant transmission modulation. In particular, by applying $180 \ kHz$ signal with peak-to-peak voltage $2 \ V_{pp}$ it is possible to achieve 80 times larger modulation around the resonance compared with the unstructured film. Although currently reported modulation depth remains small with respect to other mechanisms (0.002 % at $2 \ V_{pp}$ and up to 0.01 % at $10 \ V_{pp}$), it enables large working bandwidth from $10 \ Hz$ to $2.5 \ MHz$ for relatively small actuation voltage of $1 \ V_{pp}$. The modulation performance could be further improved by optimizing the overlap between both electric fields induced by a modulating signal and the optical illumination.

Another way to improve performance, i.e. enhancing the induced transmission modulation and reducing the voltage required for the EO-switching, is to use non-local metasurfaces supporting high-quality factor resonances. For example, quasi-bound states in the continuum (q-BIC) in lithium niobate metagratings predict high phase modulation compared to the unstructured film.[104] However, material losses and structural imperfections significantly lower the experimental q-BIC quality factor and lead to only 1.46 times larger modulation with respect to the homogeneous film. Another example of active spectral tuning of q-BIC states is realized using silicon resonators covered by a polymer with dispersed EO-molecules

(active JRD1:PMMA layer).[105] It employs second-order non-linear materials exhibiting linear EO effect as a surrounding for meta-atoms supporting high-quality factor resonances designed by the symmetry breaking. Each unit cell consists of 2 ellipses that are rotated with respect to the vertical axis, as shown in figure 3b (right). The angle of rotation allows controlling the resonance quality factor. By applying voltage, polar molecules are aligned, which changes the refractive index components, resulting in the q-BIC resonance shift, as shown in figure 3b(left). This metasurface modulates light with one of the highest switching speeds reported to date (up to 5 GHz). The authors, among other results, also reported on a voltage reduction from 100 V to 60 V by increasing the quality factor from 276 to 550.

Apart from Pockels effect, Quantum Confined Stark Effect (QCSE) creates one of the largest electro-optic coefficients (for TM-polarized light). QCSE is another enabling technology, which is used in telecommunications to designing modulators with low power consumption (up to 1 V drive) and fast operation (theoretically at sub-picosecond times).[106]

One of the best-performing metasurface using this effect has been made of patterned III-V multiple quantum-wells.[107] It is designed on a Bragg mirror to ensure near unity reflection in a considered wavelength range. Quantum well consisting of numerous doped semiconductor layers are disposed on top of the mirror and structured into double slits (Figure 3c,top). One of the dips in the reflection spectrum of this structure corresponds to a guided mode (GM) resonance coupled with the high-order multipolar resonance in quantum well grooves. This hybrid GM-multipolar resonance is located close to the wavelength of interband transition of the quantum well ($915 - 920$ nm for this structure). When the DC electric field is applied, QCSE shifts the energy levels and modifies the level of absorption, resulting in a change of a component of a complex dielectric permittivity tensor orthogonal to the layer.[108] Changing the permittivity results in the shift and broadening of a hybrid GM-multipolar resonance (Figure 3c). The second dip in the reflection spectrum in (Figure 3c) corresponds to a hybrid GM-Fabry-Perot resonance, but as it is far from the transition wavelength, it experiences only a negligible modulation. Overall, apart from the high reflection amplitude modulation due

to the hybrid GM-multipolar resonance shift (Figure 3c, bottom), metasurface introduces a phase shift up to 70 deg. The article also demonstrates a dynamic beam steering with electrical control of isolated metasurface unit elements.
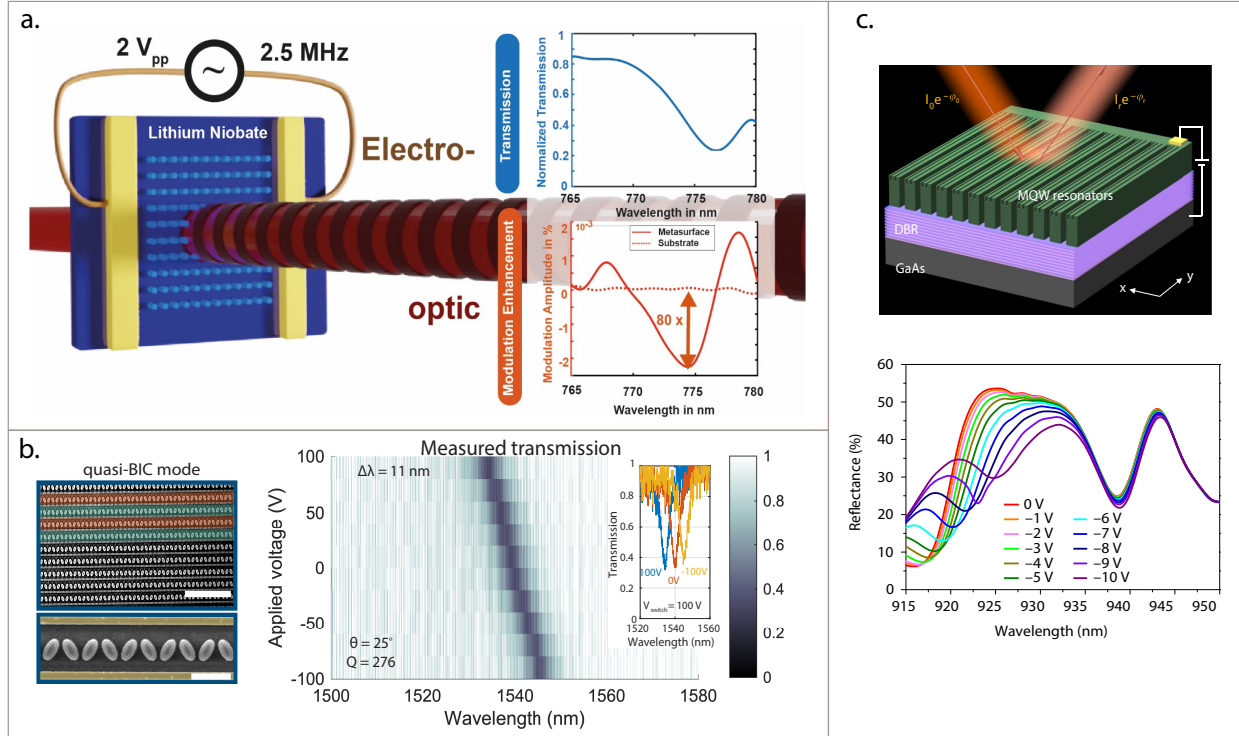

Figure 3: The electro-optic effect in lithium niobate resonators is used to achieve tunable metasurfaces with extremely interesting transmission modulation speed up to 2.5 MHz. <mark>Reprinted with permission from.</mark>[103] <mark>Copyright [2021] [ACS Publications].</mark> b. Metasurfaces consisting of quasi-BIC resonant nanoparticles producing high quality factor resonances embedded into a polymer supporting a linear electro-optic effect, also known as Pockels effect. Results demonstrate transmission amplitude modulation with a speed of up to 5 GHz. Reprinted with permission from[105]. c. Metasurface consisting of n-dopped GaAs substrate, a Bragg reflector, and a multiple-quantum-well resonators operating using quantum-confined Stark effect modulation. The bottom figure shows reflectance spectra measured at different bias voltages. It is shown that around $\lambda = 917\ nm$, for a wavelength close to the interband transition of the quantum well, the reflection modulation is considerable. with permission from.[107] Copyright [2019] [Springer Nature].

Considerable efforts were already made on the development of miniaturized thin-film electro-optic modulators and their integration into silicon-based photonic platforms have also been considered.[109–111] These modulators are based on in-plane wave propagation in waveguides, often requiring the structuring of films with standard nanofabrication techniques. In

the case of free-space modulators, miniaturization is possible with resonant metasurfaces that require nanostructuring, thus benefiting from the technology developed for waveguide EO modulators. Patterning EO materials such as lithium niobate require specific etching techniques (such as dry Ar^+ etching) and hard unconventional resists.[110] Apart from etching solid EO materials, coating polymers with organic electro-optic molecules on a nanostructured silicon platform[105] appears even less technologically challenging. Coating metasurfaces with EO materials might nevertheless complicate the pixel-by-pixel addressing issue.

2D carrier concentration modulation

Apart from relying on electro-optic effects, metasurfaces can be tuned electrically by changing the carrier concentration via electric gating. This approach, unlike EO-effects discussed previously, can be used on thin layers of standard CMOS-compatible materials which allow large-scale manufacturing. This method was attempted on various materials such as semiconductors (silicon[112] or indium antimonide[113]) but was especially successful for transparent conductive oxides (TCOs). Carrier concentration in TCOs is considerably smaller than in noble metals which allows higher changes of the refractive index under applied voltage. However, these changes remain comparatively small with respect to other tuning mechanisms. This problem can be addressed in several ways which we discuss on the example of one of the most studied TCOs - indium tin oxide (ITO).

A way to increase ITO's optical response modulation is to design ITO-based devices in an epsilon-near-zero (ENZ) regime (close to the point where the real part of the permittivity ε' changes its sign and the imaginary part ε'' is very small).[114–117] While it is hard to reach ENZ in other conductive materials due to high ε'', TCOs can easily reach this regime. Therefore, by changing the position of their plasma frequency while varying carrier concentration, larger refractive index changes can be introduced. Another approach to further increase tuning consists in summing up the response of several layers using multiple gating.[118,119] Higher modulation can also be reached by using ITO in resonant structures such as guided-mode resonance mirror,[120] hybrid plasmonic waveguide mode,[121] or resonant plasmonic antennas[122]

To mention another example of TCO, aluminum-zinc oxide (AZO) was successfully used for reflection phase and amplitude modulations in a metasurface[123]

Carrier concentration modulation is also possible in two-dimensional materials, including graphene. Since early works demonstrated tunable and highly confined plasmons in graphene nanostructures[124,125] there were many attempts to integrate them into electrically tunable metasurfaces operating in a wavelength region from mid-infrared to sub-terahertz.[126–129] Metasurfaces combining graphene with metallic antennas allow controlling reflection phase and amplitude.[126,130] Although graphene-based metasurfaces for beam-steering and spatial light modulators (SLMs) demonstrate sufficiently high phase tuning, their efficiency has to be significantly improved.[131] Another example is tunable perfect absorption in graphene-based metasurfaces[132] which is a promising result for applications requiring photon harvesting.

Despite their low efficiencies, these two modulation schemes reach high switching speeds (up to a few tens of GHz in ITO,[133] for example), making them appropriate for applications requiring fast switching such as LiDAR.[134] The combination of fast tuning mechanisms with optically engineered resonances with high-quality factors, such as quasi-bound states in the continuum, is certainly a meaningful direction to realize ultra-thin free-space modulators with a high extinction ratio.

Chemical reactions for the realization of tunable Metasurfaces

Rearranging the constituent of atoms in molecular structures, chemical reactions strongly modify the properties of materials and/or solutions. Chemical reactions can thus be of interest in adjusting the optical properties of either chemically active metasurfaces or their environments. However, this type of switching appears to be quite slow, typically on the order of seconds or more, which can be reduced to milliseconds by varying unit cell geometry and chemical reaction parameters. Being significantly slower than most of the switching mechanisms considered for fast optical modulation, chemical metasurfaces appear to be an excellent solution for niche applications such as energy-saving smart windows, or flat-panel

displays requiring operation frequency on the order of $50 - 90$ Hz.[135] Chemical tuning nevertheless has extremely valuable advantages, including room-temperature operation, low power consumption, and nonvolatile tuning. So far, several mechanisms were proposed for chemically-switched devices.

One way to introduce refractive index change of metasurface building blocks relies on a chemical reaction called hydrogenation/dehydrogenation of magnesium (Mg). When interacting with hydrogen, magnesium forms magnesium hydride (MgH_2) through a controlled chemical reaction, that switches the optical properties of the structure from metal to dielectric. By applying oxygen it is possible to reverse the transition. Considering the reaction time, switching happens within several tens of seconds to several thousands of seconds depending on the sizes of unit cells, the catalytic layer, the hydrogen concentration, and the substrate temperature. Uniform magnesium particles designed for dynamic color displays can be switched from metal to dielectric, thus progressively converting the strong plasmon resonances to weakly interacting dielectric Mie resonances until the scattering colors on the image vanish. Magnesium nanorods inducing PB-phase were used for tunable phase gradient metasurfaces,[136] or for optical signal multiplexing.[137] Applications of this effects include optical information encryption and security applications. Combined with gold, Mg nanorods were also used to create tunable optical vortices and holograms.[138]

Conductive polymers, such as polyaniline (PANI) polymer, yield another application of chemical switching in the context of metasurfaces. These are bi-stable low-cost polymers that can be electrochemically switched between oxidized and reduced forms, which induces large variations of its complex refractive index value, in particular, its imaginary part. PANI is particularly interesting for display technology, especially when combined with resonant structures that can provide even higher intensity modulation. For example, PANI can be coated on metal nanoslits for tuning the plasmon resonance wavelength,[139] or being used as a shell for plasmonic particles,[140] or even coated on plasmonic particles introducing PB-phase for beam deflection.[141] In particular, alternating coated and non-coated metasurface

sections, i.e. tunable and not tunable sections, this device produces tunable anomalous transmission with a contrast up to 860:1 (Figure 4a).[141] Phase contrast between the neighboring rows is varied inducing constructive or destructive interference which reveals or suppresses the anomalous transmission intensity. Times to induce and to reverse the process are $\approx 40\ ms$ and $\approx 35\ ms$ respectively. As discussed in the PCM section, cyclability is an important factor to consider when it comes to realistic applications. Current demonstrations reported more than 100 cycles switches. Apart from PANI, other polymers such as poly(3,4-ethylenedioxythiophene:sulfate) ($PEDOT:Sulf$) polymer network start being investigated for tunable metasurfaces.[142] The advantage of such polymers with respect to other electrochromic materials is that they can be electro-deposited and can create a thin uniform layer with well-controlled thickness.

The other mechanism of interest for chemical switching of metasurfaces employs inorganic electrochromic materials. The latter has better thermal, chemical stability, and longer durability with respect to organic materials and polymers and they are compatible with standard physical vapor deposition and lithography processes. However, their switching time is on the order of tens of seconds, limited by ionic diffusion. One of the most popular inorganic electrochromic materials is WO_3 which changes its properties depending on the type of chemical reactions. By Li^+ (or H^+) ion insertion and extraction, it transforms to Li_xWO_3 (or H_xWO_3). It has been used to make several tunable devices such as Bragg-reflector in combination with quantum dots for a tunable luminescent device[143] or core–shell structure combined with TiO_2 for smart-windows applications.[144] CMOS-compatible TiO_2 metasurfaces can be tuned by being exposed to H^+ ions. Another example of successful implementation of WO_3 for dynamic metasurfaces is shown in[145] where it is used as a spacer in a metal-insulator-metal surface producing structural color (Figure 4b). The electrochemical potential of $\approx 2V$ favors lithium insertion that changes its concentration in Li_xWO_3, resulting in a considerable refractive index change of ≈ 0.3. Device contains a Li_YFePO_4 electrode on Al collector to provide Li^+ ions. This electrode is ionically connected to a meta-

surface through a transparent solid polymer electrolyte. Applying current to electrodes, the ion-electron inter-exchange is triggered which continuously changes the scattered color by the plasmonic structures.
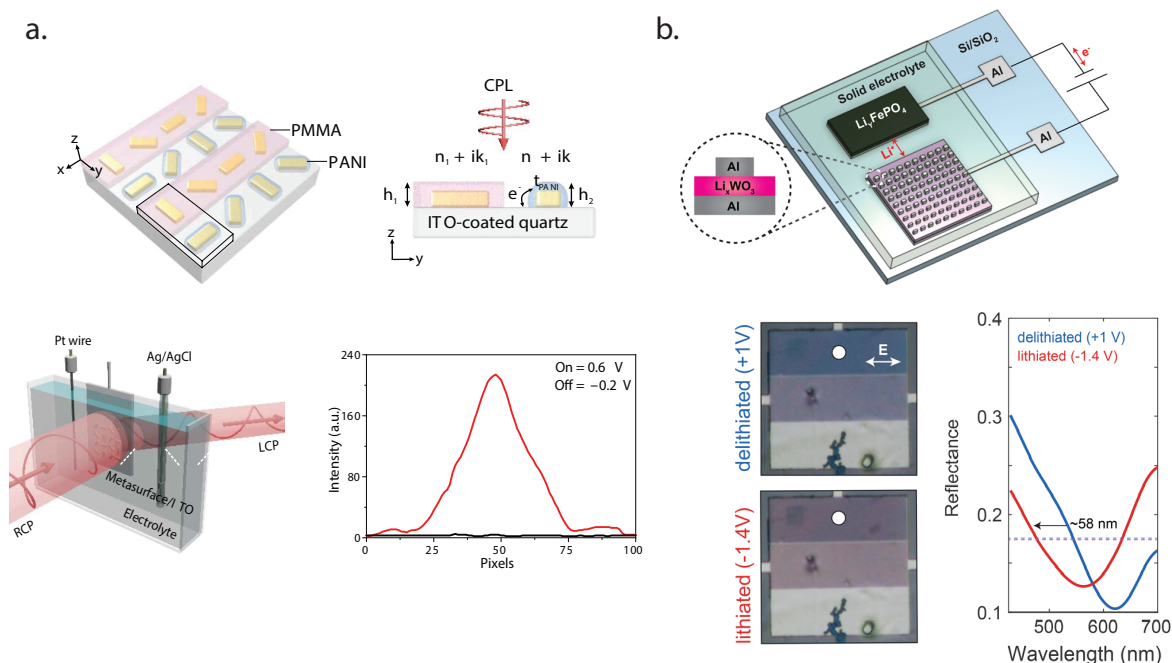

Figure 4: Chemical reactions have been considered for tuning the response of metasurfaces. a. A beam deflecting metasurface consisting of plasmonic PB-phase nanostructures is realized by coating every second row of the metastructure with PANI polymer. The latter changes between the oxidized and reduced form under applied voltage. The figure on the bottom-right shows the reported anomalous transmission intensity contrast. From.[141] The Authors, some rights reserved; exclusive licensee AAAS. Distributed under a CC BY-NC 4.0 license http://creativecommons.org/licenses/by-nc/4.0/. Reprinted with permission from AAAS. b. Schematic of WO_3 switchable metasurface by inserting Li^+ ions from a solid-state electrolyte. Lithiated and delithiated spacer in $Al/Li_xWO_3/Al$ particles is used to change the metasurface color, as shown in color-sensitive CMOS camera images. Corresponding reflectivities are shown in the bottom-right panel. Reprinted with permission from.[145] Copyright [2021] [ACS PUBLICATIONS].

Electro-chemical reactions in different electro-chromic materials were previously widely used for large volume commercial applications such as self-darkening mirrors, smart windows, and electronic displays.[146] Reducing the size of these devices down to nanoscale decreases the switching time. Meanwhile, resonant designs allow achieving full-color palette of interest for the above-mentioned applications.[139] Multiplexed metasurfaces enable polarization-control, further expanding the range of their applications to security and data protection.[137,141]

Pulling, stretching and applying mechanical stress for tuning the optical response of metasurfaces

A promising approach to dynamically address a metasurface functionality is to employ mechanical forces inducing relative motion of different parts of the device, stretching, torque, or even movement of a device as a whole.[147] Here we highlight promising works in several conventional mechanical tuning technologies such as micro-electromechanical systems (MEMS) and metasurfaces on a flexible substrate. Furthermore, we mention some novel designs such as Kirigami/ Origami-based metasurfaces and others. Extensive reviews of active mechanical metasurfaces can be found in.[148–150]

MEMS-based actuation comprises a popular solution for mechanical metasurface tuning. MEMS devices convert non-mechanical energy inputs to mechanical outputs (i.e. motion, force, torque).[151] MEMS actuators with the highest applicability are the electrostatic, electrothermal, and piezoelectric ones. Electrostatic MEMS actuators have been widely considered for metamaterial tuning.[151] They employ oppositely charged electrodes (a stationary one and a so-called membrane) separated by a tunable distance controlled by the balance between Coulomb and elastic restoring forces so as to attract the membrane towards the stationary electrode as a function of the applied voltage. This actuation mechanism is very promising for metasurface tuning since it offers a large range of motion, satisfactory speeds, low power consumption and high compatibility with solid fabrication processes.[152] A possible issue to be considered is the so-called pull-in (or snap-down) effect, corresponding to a critical value in the applied voltage beyond which elastic forces cannot compensate the electrostatic ones resulting in an unreliable motion. Another actuation approach employs electrothermal MEMS based on layered materials with different thermal expansion coefficients (TEC). Upon the application of electric currents, heat is dissipated through the structure, which expands materials differently according to their TEC. Piezoelectric MEMS have been also proposed for metasurface tuning mainly due to their low actuation voltage, low power consumption and high compactness.[153,154] In general, piezoelectric actuators undergo mechanical move-

ments according to the polarity of the applied voltage.[151] Overall, MEMS-based metasurfaces can be triggered to adopt several configurations stemming from vertical and horizontal displacements, or rotational motions of their building blocks. Their actuation speed can reach several kHz and thus it is significantly higher than that of stretchable substrates ($\sim$ 1 Hz). However, here again, pixel-by-pixel MEMS actuation of metasurface building block remains a formidable fabrication challenge, particularly in the visible domain. Several demonstrations concerning the THz and IR regime are reviewed in.[155]

If pixel-by-pixel control of the meta-atoms is challenging, an accessible solution to integrate MEMS-based metasurfaces in realistic systems consists of tuning the global optical functionalities of the components, sometimes using multi-state operation. For instance, we report on the work of Arbabi et al.,[156] where the authors have fabricated a MEMS-based varifocal metalens. Their device designed at $915nm$ consists of a doublet system, i.e. a stationary metalens and a membrane-based metalens. The membrane has mechanical resonances via attractive forces triggered electro-statically. The authors showed that a 40V actuation results in a kHz micrometric (1μm) axial displacement of the membrane causing then a $\sim$35μm shift of the focal distance. Another promising example is a tunable platform composed of a MEMS mirror combined with a plasmonic metasurface (Figure 5).[153] The fabricated device is shown in Figure 5 indicating the MEMS mirror electrically connected through the printed circuit board and the superposed metasurface. The functionalities of this compound system is activated by decreasing the distance between the metasurface and the mirror by applying a relatively small voltage of $\approx 4V$ (Figure 5 B,C). Active binary beam deflector with diffraction efficiencies of 40/46% for TE/TM polarization at $800nm$ wavelength have been demonstrated. Broadband operation of 150 nm with switching speed of $\approx 2.5kHz$ has been realized.

Flexible substrates made of soft materials like low surface energy polymers (for example, polydimethylsiloxane-PDMS) offer multiple advantages toward the demonstration of innovative metasurface-based devices with passive or dynamic functionalities.[157] For instance, their
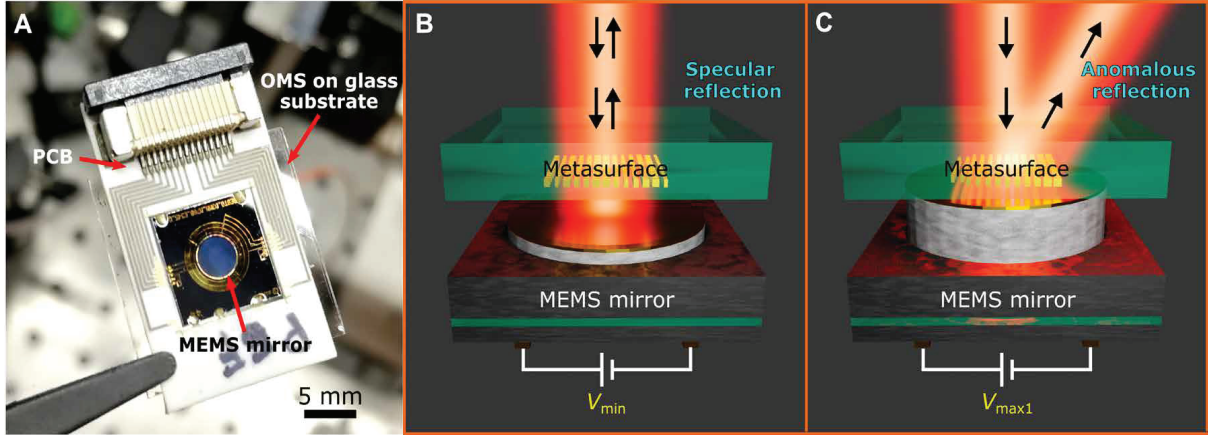
Figure 5: The performance of MEMS-tunable dielectric metasurface lens. A. Optical platform consisting of MEMS controlled electrically and a gold metasurface placed on top of the mirror on the glass substrate. B,C. Light impinging on a MEMS-metasurface compound system is manipulated to achieve the desired functionality (deflection) by simply adjusting the distance separating plasmonic metasurface and a micromirror. From.[153] The Authors, some rights reserved; exclusive licensee AAAS. Distributed under a CC BY-NC 4.0 license http://creativecommons.org/licenses/by-nc/4.0/. Reprinted with permission from AAAS.

fabrication maturity, low cost, and easy adaptation to surfaces of arbitrary shapes comprise important assets, especially considering the continuous progress of smart wearable devices for AR/VR and medical applications. Programmable contact metalenses with multi-focusing capabilities fabricated on curved surfaces to fit the human eye is only one example of the latter. Furthermore, fabricating sub-wavelength meta-atoms arrays on flexible substrates empowers conformal metasurfaces[158] and their related applications, such as cloaking, suitable for real-world implementations.[159] From the point-of-view of electromagnetic responses tunability, elastic substrates allow for the controllable and reversible strain deformations under the action of external mechanical stresses. The latter may convert the size and/or the relative positioning of the meta-units to induce phase discontinuities dynamically. An active metalens comprising of gold nanorods has been fabricated on a PDMS substrate for visible operation.[160] Mechanical stretching of the substrate changes the overall curvature of the phase profile produced by the nanoparticles, resulting in a continuous adjustment of the focal length from 150 μm to 250 μm according to stretching conditions. The authors reported on good reversibility upon sequential stretching-relaxation cycles.

24

Recently a new concept of optical nano-Kirigami/ Origami for tunable mechanical meta-surfaces was proposed.[161–163] This mechanism involves bending, cutting, folding, and twisting nano-structures that can be flexibly moved upon external stimuli actuation. One example of nano-kirigami has been realized by patterning foldable shapes on a gold film placed above SiO_2 supporting posts (Figure 6 a,b, fabricated structures are shown in Figure 6 c).[161] By applying an electric field, freely suspended patterns can be bent down forming 3D structures. Such design works in two different regimes: a broadband operation is obtained considering the structures as deformable mirrors in the regime when the wavelength is much smaller than unit-cells (geometric optics regime), while a narrow band occurs when cutting the patterns to feature optical resonances. In a former case, fabricated structures have a periodicity of $2.5\mu m$ for operation wavelengths band reaching $400 - 1000\ nm$, leading to 51% reflection modulation at the central wavelength of $750\ nm$. The switching on and off requires a comparatively high voltage of $35\ V$ (Figure 6, d). In the case of a resonant design, smaller meta-units have larger stiffness, which requires an even higher actuation voltage of $73\ V$. However, at resonant wavelength $\lambda = 1860\ nm$ reflection modulation contrast reaches 91% (Figure 6, e). In this work, modulation frequency was measured up to $200\ kHz$ and can be subject to further optimization, and, according to simulations, can reach up to $10\ MHz$. Due to their 3D geometries, origami/ Kirigami-based structures often possess helicity and chirality, making them extremely interesting for chiral bio-sensing and detection applications.[164]

Apart from the mechanisms mentioned in this section, several emerging designs with high potential are on the way. For example, cross-stacked nanoparticle chains have been fabricated using colloidal assembly and have been showing large tunable circular dichroism of interest for chiral sensing.[165] Another example is the recently demonstrated meta-vehicle consisting of passive metasurfaces steered along the surface of a fluid using optical forces and torques.[147]

Mechanically-actuated meta-optics systems are certainly promising and would partici-pate in further advancing the field of space-time metasurfaces in the coming years. Devices
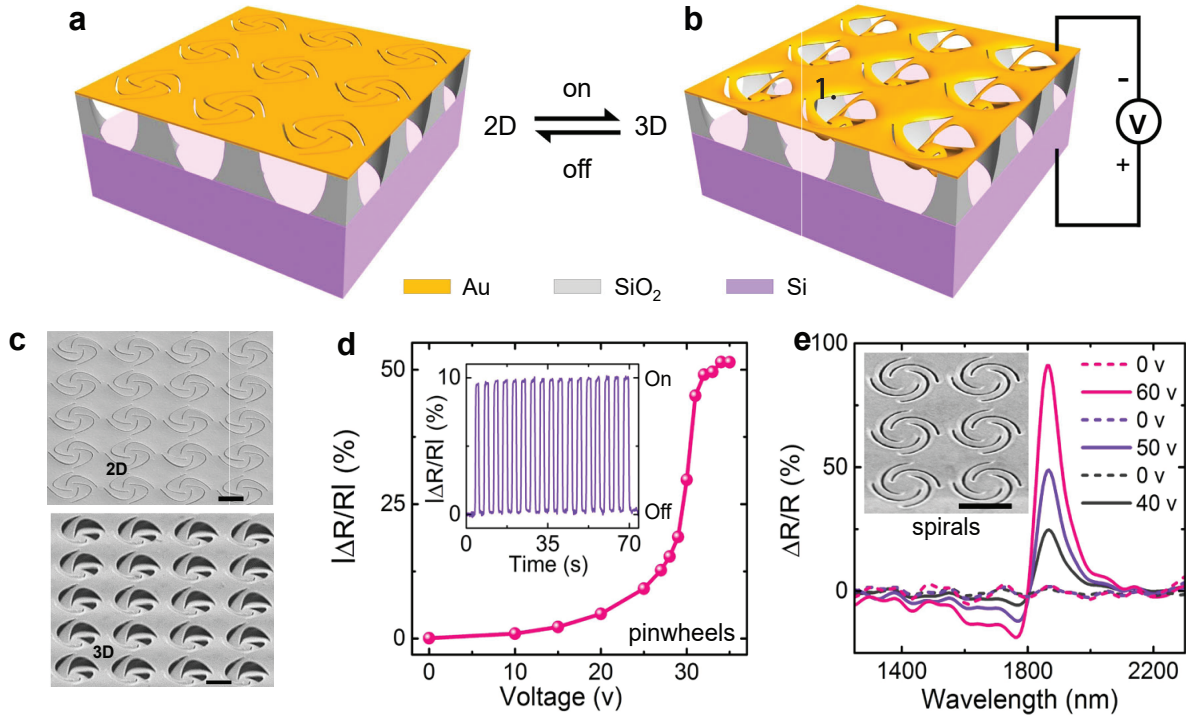
Figure 6: Mechanical tuning of Kirigami-metastructures to modulate the reflection of light. a,b. Schematic representation of a Kirigami-Metasurface. Tuning the geometries of the gold pinwheels from 2D to 3D is realized using electrostatic forces applied between the gold film and the underlying substrate. Downward folding of suspended structures is permitted by under-etching a thin layer of SiO_2, creating supporting edge pedestals around the folded elements. c. Scanning electron microscopy images of fabricated metasurfaces from (a,b) d. Amplitude contrast of the reflectivity at different voltages for a kirigami-metasurface much larger than operation wavelength. Inset highlights the On/Off reliable cyclability of the reflection amplitude modulation e. Response of resonant Kirigami-Metasurface showing reflection amplitude modulation around resonant wavelength for different applied voltages. Reprinted with permission from.[161] Copyright [2021] [Springer Nature].

such as MEMS possess a high degree of technological maturity and they are particularly attractive due to their compatibility with the CMOS manufacturing process and their noticeable modulation performances. For example, thin-film piezoelectric MEMS can achieve up to 30 MHz modulation frequency,[153] high cyclability (up to 10^{11} cycles at 20 V cycles),[166] and operate at room temperature. Pixel-by-pixel MEMS actuation remains challenging but solutions to break the structural symmetry in the out-of-plane (third) dimension have been explored in the visible domain as mentioned above, but also at THz and microwave frequencies.[167] Efforts in addressing individual building blocks at visible wavelength are nevertheless still needed. Apart from standard technologies, suggested novel designs have a high potential

for industrialization due to their mass-production simplicity.[165]

Pushing the limits of Liquid Crystals light modulators towards active and adaptive meta-optics

Thermotropic Liquid Crystals (LCs) or in other words mesophases appearing between the crystalline solid and the isotropic liquid phase with temperature change,[168] have a long-term tradition in electro-optical devices.[169] Indeed, LCs represent a dominant technology in the display industry but they have also proven their power in non-display programmable devices such as lenses, spatial light modulators, and beyond.[170] It was inevitable that LCs would attract the interest of the meta-material (-surface) community due to their formidable physical properties, their responsiveness to external perturbations, and their technological maturity. Some relatively early works introducing LCs for metamaterial tuning can be found in.[171,172] Among the different identified LC phases, it is the so-called "Nematic", that was placed in the foreground for metasurface tunability. Nematic LCs (or NLCs) present strong shape anisotropy at the molecular level leading to long-range orientational order without translational one. Interestingly, NLCs have orientation-dependent properties such as considerable birefringence (Δn- typically between 0.05 and 0.45), while at the same time they are fluids. NLC average molecular orientation (or "director") is vulnerable to various stimuli including electric and magnetic fields, light, temperature, and mechanical stresses offering large tuning flexibility depending on the targeted application. By re-orienting the director with respect to light's k-vector one can select the NLC refractive index experienced by the incident polarized light. To this end, NLCs have been mainly used to dynamically shift the resonances of plasmonic and dielectric metasurface building blocks known to be very sensitive to variations of their optical surrounding. In several demonstrations, an in-plane to out-of-plane switching is used, where the angle between the director and the light's wavevector defines the refractive index and leads to electrically controlled birefringence (ECB). It holds that

$n_e(\theta) = \frac{n_e n_o}{\sqrt{n_e^2 \cos^2\theta + n_o^2 \sin^2\theta}}$, where n_e is the extraordinary refractive index, n_o the ordinary one, θ is the angle between the director and the light's k-vector and $\Delta n(\theta) = n_e(\theta) - n_o$ is the ECB. The previous relationships show that NLCs can be used for both binary ON-OFF switching, but also to induce continuous refractive index gradients. The latter, constitutes the basis of NLC-SLMs operation.[173] Electrically triggered NLC metasurfaces have been also used to control the polarization of the light in twisted-Nematic cells known to induce optical activity.[174] For any NLC alignment, when the voltage is sufficiently increased, an NLC with positive (negative) dielectric anisotropy will tilt towards (perpendicular) the electric field's direction so as to minimize its free energy. The mechanism behind the electrically-induced NLC reorientation involves the competition between electric, elastic, and anchoring forces. The latter describes the formation of a specific director's orientation at the interfaces between the LC and solid substrates that confine the anisotropic fluid in practical applications. We highlight here that NLCs are very attractive to metasurfaces since they respond to few volts (usually 1-5V), they possess broadband birefringence, as well as they present small or negligible losses in wide spectral windows. All-optical metasurface tuning has been also successfully demonstrated showing the versatility of NLC responsiveness.[175,176] It is interesting that NLC's fluid nature allows straightforward infiltration into pre-fabricated passive metasurfaces serving at reducing cost and complexity.

Independently of the employed stimulus, NLC addressable metasurfaces have already shown their large potential for several applications including varifocal metalenses (see for instance figure 7 a.),[177] spatial light modulators,[178] projection displays,[179,180] sensors,[181] thermal camouflage[182] and so on. Moreover, devices operating at different spectral regions show the flexibility in adapting conceptualized operation principles at different frequencies ranging from microwaves to visible.[178,183–185] However, except for the obvious advantages, there are still reported constraints that need to be tackled. We find it useful to direct the following discussion towards two axes that have to be carefully considered for the realization of NLC-tunable metasurfaces. These are: **- the control of NLC alignment at the**

metasurface vicinity, - the improvement of the NLC response time in case of electrical tuning.

Homogeneous NLC alignment before the application of any perturbation is critical in LC-based applications since it ensures a high degree of order that maximizes the optical anisotropy. NLC anchoring condition at the interfaces with other materials is very sensitive to the NLC properties as well as to the chemical composition and the structure of the underlying surface. In LC displays, the anisotropic fluid is confined between glass substrates covered with transparent electrodes and alignment layers. The existence of such layers ensures a uniform director's field before the voltage application. Alignment coatings are usually created by either mechanical rubbing or photo-alignment. However, when the NLC is infiltrated into a sub-wavelength structured environment, such as a metasurface, imposing a particular alignment condition is not a trivial task. Several groups have reported on the issue of NLC's poor alignment close to metasurfaces while others adopted strategies to prevent or eliminate this issue. Sun et al. discussed the importance of the anchoring condition of the NLC mixture E7 at the vicinity of a TiO_2 dielectric MS composed of 190 nm thick cylindrical structures (Fig. 6b.)[186] In that work, a 1.5μm-thick E7 cell is sandwiched between the metasurface fabricated on the top of an ITO layer and a top window covered with a second electrode. Then a voltage application causes bulk NLC reorientation to modify the refractive index and thus to tune the metasurface resonances. To ensure the uniform in-plane orientation of the NLC molecules at VOFF state the authors use photo-alignment for the cover window. However, they found that there is a deviation angle between NLC alignment close to the metasurface and the photo-alignment direction. By considering the NLC free energy expansion and using an Euler-Lagrange minimization process they explained that the anchoring condition close to the meta-structures is strong-enough to dominate over the photo-alignment direction. An even more decisive alignment strategy has been suggested by Su et al.[187] encompassing mechanical rubbing at the upper window but photo-alignment treatment at the bottom metasurface. Nevertheless, the authors highlighted the importance

of the metasurface topography upon the NLC molecules orientation close to the meta-atoms. In their recent publication Lininger et al. presented experimental results showing the impact of NLC director inhomogeneities on the optical response of infiltrated metalenses.[188] Dolan et al. discussed the effect of NLC radial disordering around cylindrical pillars on the optical near fields of TiO_2 metasurfaces in the visible range and proposed numerical simulation strategies for accounting for these phenomena.[189] They among others emphasised the emergency of optically simulating the NLC via its dielectric permittivity tensor especially when the disorder is present close to the metasurface building blocks. In the latter publication, vertical alignment of the NLC molecules has been considered by chemical functionalization of the metasurface and the upper window by octadecyltrichlorosilane (ODTS) in heptane solution. Chemical treatment seems to reduce the complexity in terms of fabrication compared to mechanical rubbing and photo-alignment since it may be applied to the metasurface as a post-fabrication process. Moreover, it can be employed to control the anchoring strength of the NLC layer immediately adjacent to the metasurface accounting also for the metasurface fragility. In the presence of very strong anchoring, the NLC molecules at the near field of the meta-units will not respond to the external field. This issue can be controlled by relaxing the anchoring forces close to the metasurface.[190] The reduction of the metasurface substrate contribution has been also proposed as a solution to moderate anchoring forces close to the meta-atoms.[191] NLC director is very sensitive to the geometries of other materials placed in its vicinity. Generally, it is anticipated that structures generating an anisotropic environment compatible with the NLC molecular shape will lead to enhanced alignment. For instance, grating-like metasurfaces could be an alternative[192] compared to cylindrical pillars generally reported to be associated with local NLC disorder.[192] Finally, high aspect ratio structures have been proposed for NLC vertical alignment.[193]

The use of NLC metasurfaces for realistic applications requiring ultra-fast, real-time tunability is a great challenge. For instance, beam steering devices that could be used as laser scanners for LiDAR systems require scanning frequencies on the order of MHz.
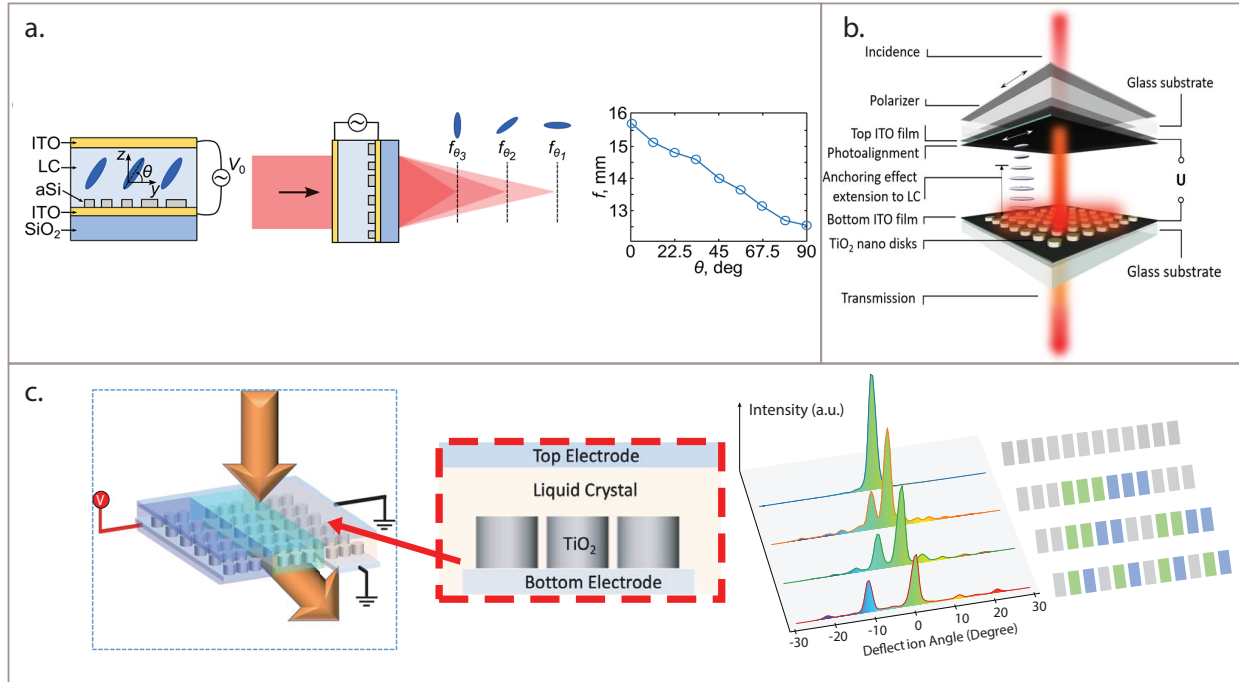
Figure 7: Tunable metasurfaces infiltrated with liquid crystal molecules. a. Si-based metal-ens encapsulated with NLC. By changing the LC reorientation angle electrically, a varifocal function has been demonstrated. Reprinted with permission from.[177] Copyright [2021] [ACS PUBLICATIONS]. b. Electrically addressable transmissive device based on TiO2 metasurface infiltrated with an NLC. At V_{OFF} state the NLC is aligned along the photoalignment direction imposed at the cover window. Asymmetric alignment is established at the different cell sides. Due to the strongest anchoring at the metasurface side, the bottom alignment condition is dominant in the cell.Reprinted with permission from.[186] Copyright [2019] [Nature Publishing Group]. c. Phase-only SLM in transmission based on a TiO_2 metasurface tuned by an NLC. The device is composed of pixelated bottom electrodes each having three TiO_2 nanopillars on the top. A common upper electrode is considered for the voltage application. The device is infiltrated with an NLC tuned at three voltage levels (blue-green-gray) along the sequential electrodes to deflect the incident beam. A maximum deflection angle of 11° has been demonstrated. Adapted with permission of AAAS, from;[178] permission conveyed through CCC, Inc.

.

Electro-optical devices based on NLCs are known to exhibit millisecond switch-on (τ_{ON}) and relaxation (τ_{OFF}) responses ($\tau_{ON} < \tau_{OFF}$). kHz speed is adequate for display applications due to the human eye's perception capabilities, but it is too slow for more demanding applications including LiDAR scanning. NLC voltage-response time is dictated by the intrinsic physical properties of the employed molecules (i.e. the elastic constants, the rotational viscosity, the dielectric anisotropy) as well as by the temperature, the anchoring strength, and the distance between the electrodes. For a given NLC molecule, the switching time is proportional to the square of the distance between the electrodes. Typical phase-only LC-SLM devices employ

planar electrodes confining an NLC layer. The top electrode usually acts as a reference, while the bottom one is pixelated to induce gradual 2π phase retardation to the process of light propagation. Since the phase retardation is exclusively accumulated into the NLC layer, the distance between the electrodes is at least of few microns for visible wavelengths and typical Δn values. Moreover, these conventional SLMs targeting visible applications, are fabricated with micrometric pixel pitch that leads to low deflection angles, multiple diffracted orders, and reduced efficiency. In their work, Li et al. reported on uncoupling phase modulation from NLC thickness by using a Huygens dielectric metasurface, where the main phase accumulation happened inside the TiO_2 nanopillars.[179] The latter is of particular interest not only for faster beam steering but also to moderate pixel crosstalks, unavoidable in bulky LC cells. The authors demonstrated an NLC metasurface beam steering device in the visible range with a maximum deflection angle of 11° and 36% efficiency in transmission (Fig. 6c.). Other reported approaches for enhancing both τ_{ON} and τ_{OFF} have proposed dual-frequency LCs known to change the sign of their dielectric anisotropy according to the frequency of the applied electric signal.[194] A particularly promising approach for speeding up the LC response time has been proposed in a recently released patent introducing LC metasurfaces operating in reflection mode as a valuable solution for ultra-compact LiDAR systems.[195] In this patent, the authors propose the employment of metallic vertical (instead of planar) electrodes to electrically activate the LC infiltrated between them in a tiny (sub-wavelength) volume. The electrode distance reduction speeds up the LC response time to a few tens of microseconds. Interdigital electrodes have been also discussed in the recent past as a solution for achieving sub-millisecond responses.[192] However, by also extending the height of the electrodes over the whole device thickness one enhances electric field uniformity and eliminates inter-pixel crosstalks in pixelated programmable metasurfaces.

Finally, we are questioning if the maturity of LC technology is enough to follow the continuously increasing demands of tunable metasurface applications? As explained in the previous paragraphs the principal reported challenges in LC-metasurface technology are

dealing with the ability to control the alignment properties at the metasurface environment and to enhance the NLC time-responses. The recent advances revealed that these problems can be tackled by reconsidering novel device architectures with dedicated alignment procedures. To this end, we believe that the strong industrial activities around LC electro-optical devices would help LC-tuned metasurfaces to access the market faster than the other solutions discussed in this report. However, we highlight that efforts are needed not only from the metasurface but also from the LC scientific community. For instance, novel NLC molecules with improved physical properties and LC phases beyond Nematic (Smectic and Blue phases) could be investigated to further improve their integration with metasurfaces. The employment of ferroelectric LC phases known to exhibit microsecond responses could be an alternative for fast switching.[196]

Perspectives

In this article, we selected among the most promising approaches reported so far for applications requiring real-time and programmable light manipulation with planar metasurfaces. Our selection criteria encompass the level of readiness of the technology to penetrate the industrial market, the complexity in terms of design and fabrication, the reported performances, and the device reliability. Up to now, research efforts devoted to metasurface tunability mainly propose materials that adapt their optical properties to external agents including electric fields, light, temperature, and mechanical forces. These materials can be either used for sub-wavelength building blocks or the tunable optical environment for intrinsically passive meta-units. The various mechanisms for metasurfaces tuning that have been demonstrated exhibit different performances and properties. Therefore, one can select among the different available mechanisms according to the targeted application or equivalently to the performance. As an example, electro-optic materials are good candidates for hybrid photonics complementing silicon-based platforms due to exceptionally high mod-

ulation frequencies typical for these materials, generally in the GHz regime.[109] NLC and chemically-tunable metasurfaces are more promising for display applications due to their low-voltage operation, relatively low addressing speed, and comparatively low cost. More application possibilities are summarized in Table 2 by considering the individual advantages of each tuning mechanism. Interestingly, the apparent limitations of a given modulation mechanism can be turned into significant advantages. For example, the extremely large optical losses of GST material could be utilized for applications requiring fast programmable amplitude modulation.

If current efforts on tunable metasurfaces concern mainly academic research, the continuously growing industrial interest for dynamic, ultracompact and integratable optical components demands the quick laboratory-to-market transition. The synergy between different scientific and technological disciplines spanning physics, chemistry, nanotechnology, electrical engineering and computer science is the key to speed-up the process for bringing dynamic metasurfaces ready to market applications. CMOS (Complementary Metal Oxide Semiconductor) technology, being the cornerstone for manufacturing micro and nanodevices, is considered for mass production of dynamic metasurfaces, such as Lumotive example that co-fabricate LC metasurfaces with Himax semiconductor specialist. ST microelectronics, a world-leader for MEMS and PCM memory industrialization, could play a significant role in the industrialization of PCM metasurfaces. Electrical tuning (which is clearly the most promising and the most practical modulation technique) architectures remain complex requiring pixel-by-pixel voltage application bridging sub-wavelength features with large scale electronic driving board. Commercially available display drivers exploiting the similarity with the highly mature LCD technology would be useful to speed up the market readiness of LC actuated metasurfaces, but customization of the electronic architectures to enable individual control of the meta-atoms by field-programmable gate arrays (FPGA) is inevitable. The development of advanced algorithms to program the designed optical functionalities in real-time is still needed. These algorithms are of interest to perform dynamic post-fabrication

optimization aiming at maximizing the performance of tunable metasurfaces. Post-process optimization is generally not achievable with passive metasurface counterparts. In their recent review, Tsilipakos et al.[197] discuss the possibility of software-defined metasurface networks that enable intra-communication as well as interaction with the external environment by user-friendly interfaced applications. Systems embedding one or several metasurfaces will thus be considered in the future for various applications consistent with the terms IoT and AoT.

Tuning mechanism	Illustration	Advantages	Bottlenecks	Applications
PCM		• Large Δn • non-volatile Chalcogenide PCM • material options with low losses • multi-state operation • high/ medium cyclability • fast switching: up to kHz for metasurfaces (10 kHz in[90] for GST), up to 10 MHz for optical memory[198]	• non-uniform heating • cooling that limits switching speed • High losses in VIS and NIR for GST	• non-resonant components for broadband applications due to large Δn • fast-speed application for optimized structures • Non-volatility enables optical neuromorphic applications[199]
Electro-optic effect		• Fast switching (up to 5 GHz)[105] • Low power consumption • High cyclability • High transparency in VIS	• Small index change	• High-speed communication and computing
Chemical tuning		• Cheap/facile to fabricate polymers • Bi-stability • Low power consumption ($\approx 1V$) • Continuous tuning • room temperature operation	• Slow switching ($\approx$ $10ms$ − $1000s$)	• Slow modulation applications including electronic displays and smart windows • Security and data protection[137,141]

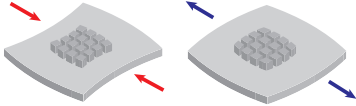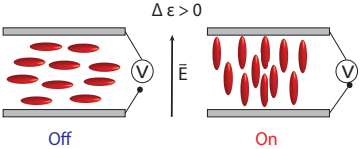|		Advantages	Bottlenecks	Applications
Mechanical tuning		• Optical contrast provided by geometry tuning • Fast switching (up to 100 kHz) • Power consumption can be less than 20 mV • MEMS- and CMOS-compatible	• Difficulty of scaling down • Low lifetime for stretchable substrate • Constraint imposed by moving parts	• Switchable lenses or deflectors for free-space optical tracking /communication[153] • Chiral sensing[165] • Spectral modulation[200]
Liquid Crystals		• High transparency in several spectral regimes including VIS • Straightforward infiltration due to fluid nature • Low-cost materials • Low power consumption • response at low voltages $\approx 1 - 5V$ • ON-OFF and continuous tuning • room temperature operation • Highly mature technology	• polarization dependency • sensitivity to MS topography • slow switching in bulk devices	• Displays • Next generation of compact LiDARs[195] • Fast optical interconnects

Table 2: Table comparing five selected tuning mechanisms considering their advantages, bottlenecks, and highlighting examples of possible applications

Addressing not only fast but ultrafast light modulation, on the order of a fraction of the optical frequency, offers new interesting academic perspectives in particular with the emerging topic of space-time metasurfaces. Spatio-temporal control of electromagnetic waves extends the realm of functionalities enabled by the conventional tuning mechanisms explicitly discussed above In particular, breaking time-reversal symmetry might be interesting for the realization of a new class of non-reciprocal optical systems. A discussion explaining the physical mechanisms and solutions currently studied at the academic level, including the use of bianisotropic metasurfaces is provided.

In the introduction, we mentioned that the foundation of optical metasurfaces obeying the generalized laws of reflection and refraction[17] consists in modifying the tangential momentum of light upon reflection and transmission. New degrees of freedom leading to broader versions of these laws can be induced by considering the temporal dependency of these phase gradients.[201] Space-gradient-only metasurfaces are restricted by Lorentz reciprocity and are thus called reciprocal **A system is defined as reciprocal when the ratio of the received to the transmitted field is not changing as one exchanges the transmitter and the receiver.**[202,203] Usually, reciprocity is defined by symmetry in the electromagnetic trajectory upon time-reversal. Time reversal symmetry is thus equivalent to reciprocity when: **(1)** the trajectory corresponding to the original forward process coincides with the time-reversed trajectory and **(2)** the absolute amplitude of the originally transmitted field is equal to the amplitude of the received field upon time-reversal. For a loss-(gain-)less system **(1)** and **(2)** both guarantee reciprocity and time reversal symmetry. However, in a lossy system time-reversal symmetry is broken due to the violation of **(2)**. For instance, as light travels through a lossy metasurface, its amplitude decreases, and as it travels back in a time-reversed scenario, it decreases even more but by the same percentage. This metasurface is reciprocal because the ratio of the received to the transmitted field is the same for forward and backward propagation directions (symmetry in terms of field ratios), but the time-reversal symmetry is broken, because the absolute field amplitudes are different (asymmetry in terms of absolute fields).[203] Very good and comprehensive tutorials discussing in detail the different aspects of time-reversal symmetry breaking and other notions concerning the reciprocity concept are available in the literature.[203–207]

Breaking reciprocity for electromagnetic waves would mean realizing components such as diodes, optical isolators, and circulators, i.e. devices generally providing asymmetric responses.[208] However, using a structurally asymmetric device wouldn't be sufficient for non-reciprocal devices since time-reversal symmetry should also be broken. The conventional way to break time-reversal symmetry encompasses the employment of magnetic materials

triggered by internal or external magnetic fields. However, these materials exhibit limited applicability especially at optical frequencies stemming among others from their bulkiness, losses, cost, and integration inconvenience. Magnetic-free approaches are therefore highly desirable for opening the way for the demonstration of non-reciprocal components.

Non-linear metasurfaces have also been proposed as magnetic-free solutions to break reciprocity.[209] These materials present optical responses that are dependent on the applied electric field intensity. In particular, the proportionality of the coefficients between the polarization the non-linear field terms are the high-order susceptibility tensors leading, according to their order, to prominent non-linear effects such as the Kerr effect, second (third) harmonic generation - SHG (THG), etc. Non-linear metasurfaces require very high light intensities that are not always desirable in practical applications due to inconvenient power requirements.

During the last years, the focus for breaking time-reversal symmetry accompanied with multiple-harmonic generation was concentrated around the temporal modulation of different metasurface properties. One of the pioneering works introducing space-time metasurfaces is that of Hadad et al.[210] To this end, several other efforts have been dedicated to the conceptualization and the demonstration of time-varying metasurfaces.[211–213] In practice, controlling the metasurface functionalities in time is not an easy task especially when considering ultra-fast modulators. This can be achieved in the microwave regime for instance by employing varactor and PIN (positive-intrinsic-negative) diodes. Just to mention some interesting concepts and/or demonstrations, Zhang et al., proposed space-time-coding metasurfaces to isolate reflections in the space and the frequency domain, controlled by PIN diode programmed by digital codes.[214] They experimentally verified non-reciprocity in the frequency domain. Liu et al. suggested a time-varying Huygen's metasurface for parametric wave scattering at microwaves using varactor diodes as tunable elements.[215] The authors supported their concept by experimental results and among others claimed that their idea could be brought at optical frequencies by exploiting modulation mechanisms such as electro-optic

and acousto-optic effects. Very recently, the concept of a non-reciprocal electromagnetic isolator has been presented, supported by numerical results introducing a space-time coding metasurface based on electronic rotational Doppler shifts.[216] In figure 8 we provide a simplified illustrative example presenting wave-engineering capabilities achieved by space-only, time-only, and space-time discontinuities. Figure 8a. presents the general wave-scattering process of an incoming plane wave (I) $\vec{E}^I(\vec{r},t) = \vec{A}e^{i(\vec{k}\vec{r}-\omega t)} = \vec{A}e^{i\phi(\vec{r},t)}$, where $A = |\vec{A}|$ is the amplitude and $\phi(\vec{r},t)$ is the phase, when it encounters spatial, temporal and spatiotemporal discontinuities in the optical density of a medium. The phase depends on both spatial and temporal coordinates, where $k = |\vec{k}|$ is the wave number composed of a transverse momentum $k_\parallel = k_x$ and ω is the frequency. Particularly, as progressively illustrated in 8a. from the top to the bottom, the incident wave impinges on a spatial, a temporal and a spatiotemporal boundary separating two different optical media of refractive index n_1 and n_2 respectively. In the space scenario, the boundary is placed at a particular position z_o of the space coordinate axis, where n_1 corresponds to $z < z_o$ and n_2 to $z > z_o$. In such a case, the incident wave (represented by an orange arrow) will be partially reflected back in the medium n_1 (black arrow - R holds for reflection) and partially refracted in the medium n_2 (purple arrow - T holds for transmission), as described by Snell's law. Crossing the spatial boundary, the beam will not change its frequency due to energy conservation. However, the total momentum changes to account for the refractive index change given the dispersion relation $k = \frac{\omega}{c}n$, where c is the speed of light in vacuum. The momentum in the second medium is equal to $k_2 = \frac{n_2}{n_1}k$, where k is the incident wave number, while the reflected wave is propagating along -k. In the temporal scenario, the refractive index changes from n_1 to n_2 at a particular moment in time and for all the positions in space, which is equivalent to splitting two media with refractive indices n_1 and n_2 at a temporal interface t_o. As illustrated in 8a. middle panel for $t < t_o$ the refractive index is n_1 and for $t > t_o$ it is n_2. A wave travelling in the $t < t_o$ regime is an earlier wave compared to the later waves occurring for $t > t_o$. In this scenario the momentum carried from the light travelling forward in the medium n_2 (purple arrow) is conserved but

the energy is not. The second panel of 8a. describes what is called "time refraction" and it can be perceived as the temporal counterpart of the conventional Snell's law leading to the frequency shift of the refracted beam. A wave travelling later backward in time, imposing a time reversed scenario where $t \to -t$ holds for the time reflected wave (black arrow). Note that the absolute value of the frequency change of the transmitted and the reflected waves in the second medium ($|\omega_2| = \frac{n_1}{n_2}\omega$) is the same for both waves as it depends only on the optical densities of the two media. In figure 8a. (middle), we denote the time reversed reflected (R) wave with a negative sign in front of the frequency so as to indicate that the propagation occurs in the later backward direction in time. The bottom panel in the 8a. corresponds to the general case where a spatio-temporal boundary separates the two media n_1 and n_2. A wave crossing such a boundary will change both its frequency and momentum as indicated by (k', ω'). The two black arrows in figure 8a. bottom panel show that the reflected beam can propagate either in the medium n_1 (dashed arrow) or in the medium n_2 (solid arrow) depending on the velocity of the interface. Particularly, if the interface moves slower than the speed of the light (sub-luminal case), the wave will be reflected inside the medium n_1, while it will be reflected inside the medium n_2 when the velocity exceeds c (super-luminal case). [206,217]

After introducing the different spatiotemporal boundaries, we could now discuss cases of time modulated nanostructured interfaces, leading to Doppler-like frequency conversions, breaking both time reversal symmetry and reciprocity as introduced in. [201] Let us consider the case of a metasurface that induces phase discontinuities on reflected and transmitted fields. Here, we consider reflection only in an optical medium n for simplicity. These phase discontinuities we are considering hereafter can be induced in space and/or in time over a fixed spatial period along the x-direction with a uniform temporal modulation, i.e. considering only the same frequency modulation for all the elements of the period. For an obliquely injected plane wave at the metasurface, $\phi(\vec{r}, t)$ is representing the spatial and the temporal phase evolution. Its frequency can thus be written as $\omega = -\frac{\partial \phi(\vec{r}, t)}{\partial t}$ and its transverse wave

vector along the x-direction as $\vec{k}_x = (\frac{\partial \phi(\vec{r},t)}{\partial x})\hat{x}$. Spatiotemporal modulation adds an extra tangential momentum $\Delta k_x = \frac{d\phi(x,t)}{dx}$ and shifts the frequency of the incident wave by a factor $\Delta \omega = -\frac{d\phi(x,t)}{dt}$. Under such a consideration, the phase of the reflected wave can be expressed in terms of its wave number and its frequency given by:

$$k_{R,x} = k_{I,x} + \Delta k_x \Rightarrow k_R \sin \theta_{R,t\to+t} = k_I \sin \theta_{I,t\to+t} + \Delta k_x \tag{1}$$

$$\omega_R = \omega_I + \Delta \omega = \omega + \Delta \omega \tag{2}$$

In the relationships (1)-(2) the subscripts I, R correspond to the incident and the reflected wave respectively, while the notation $t \to +t$ shows that the time moves forward. Combining equation (2) with the dispersion relation $k = \frac{\omega}{c}n$, we have:

$$k_R = \frac{n}{c}(\omega + \Delta \omega) \tag{3}$$

Due to (3), the relationship (1) brings the spatiotemporal version of the generalized law of reflection, written as:

$$\sin \theta_{R,t\to+t} = \frac{\omega}{\omega + \Delta \omega} \sin \theta_{I,t\to+t} + \frac{c}{n(\omega + \Delta \omega)}\Delta k_x \tag{4}$$

Similarly, we derived the generalized space-time Snell's law, leading to:

$$\sin\theta_{T,t\to+t} = \frac{n\omega}{n_2(\omega + \Delta\omega)}\sin\theta_{I,t\to+t} + \frac{c}{n_2(\omega + \Delta\omega)}\Delta k_x \tag{5}$$

The subscript T in (5) refers to the transmitted wave, while n and n_2 are the refractive indices of the incident and the transmitted medium respectively.

Now we consider the reflection cases of space gradient and time modulated metasurfaces independently.

Space-only modulated metasurface: for a pure space gradient ($\Delta k_x \neq 0$) we substitute $\Delta\omega = 0$ in (4). We get:

$$\sin\theta_{R,t\to+t} = \sin\theta_{I,t\to+t} + \frac{\lambda}{2\pi n}\Delta k_x \tag{6}$$

As expected, equation (6) describes the generalized law of reflection,[17] where λ is the free-space wavelength. Now let us suppose that a wave is impinging on the space-only gradient metasurface at an angle $\theta_{I,t\to-t} = \theta_{R,t\to+t}$, mimicking a time-reversed scenario where $t \to -t$, as in practice time cannot be reversed. In such a case, $\phi(x)$ is constant in time and $\Delta\omega = 0$. Substituting $\Delta\omega = 0$ in (4) and replacing $\theta_{I,t\to+t}$ by the time reversed incident angle $\theta_{I,t\to-t} = \theta_{R,t\to+t}$, we find that the reflected wave in the time reversed scenario leaves the metasurface at an angle $\theta_{R,t\to-t} = \theta_{I,t\to+t}$, subtracting thus a tangential momentum Δk_x from the incident wave. To summarize, in the time-backward process, the reflected beam from a spatially-only modulated interface reflects at the same angle as its conjugate ($t \to +t$) in the time-forward process, which is the definition of reciprocity. The process is illustrated schematically in the top panels in 8b. and 8c. Particularly, in 8b., the process is represented by horizontal wave number transitions in (k_x, ω) space for both $t \to +t$ and $t \to -t$, resulting from the energy conservation restriction for space-only modulated metaurfaces.

Time-only modulated metasurface: we call time-only modulated metasurface an
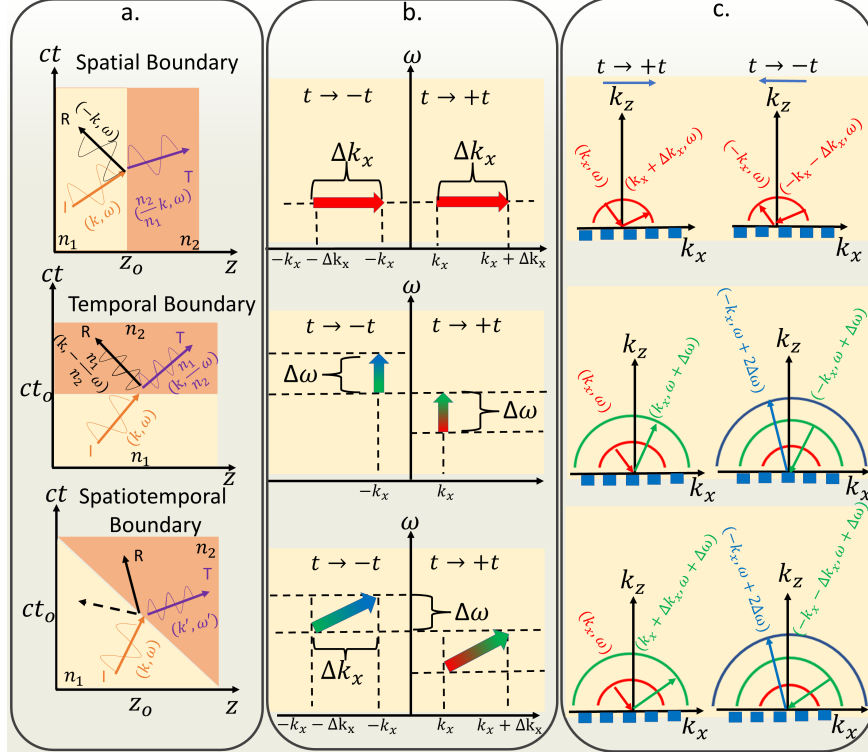
Figure 8: a. Top to bottom panels illustrate the wave scattering process from a spatial, a temporal or a spatiotemporal boundary separating two media of refractive indices n_1 and n_2 respectively. In all the panels I, R and T hold for the incident, the reflected and the transmitted wave, represented then as orange, black and purple arrows respectively. The incident wave has always a momentum k and a frequency equal to ω. b-c. An example showing a space-, a time-, and a space-time modulated reflective metasurface (from top to bottom in both b. and c.). Particularly b. presents the frequency and the tangential momentum transitions upon reflection for both forward ($t \to +t$) and time-reversed ($t \to -t$) propagation. A space-gradient along x-direction is considered in 8b. top and bottom panel, providing an extra tangential momentum $\Delta k_x > 0$ for both $t \to +t$ and $t \to -t$, thus adding (subtracting) Δk_x upon forward (time reversed) propagation. The temporal modulation in the middle and the bottom panel up-converts frequency for both $t \to +t$ and $t \to -t$ cases. The solid filled red arrow in 8b. top panel represents horizontal momentum transitions without frequency change for space-gradient only. The gradient filled arrows in 8b. middle and bottom panels show that the vertical and the oblique transitions for temporal and spatiotemporal modulation are accompanied with frequency shift without or with tangential momentum change respectively. Fig. 8c. shows the $t \to +t$ and $t \to -t$ trajectories of a wave interacting with a spatially (top), a temporally (middle) and a spatiotemporally (bottom) modulated reflective metasurface. The red, green and blue semicircles represent iso-frequency curves corresponding to $\omega, \omega + \Delta\omega, \omega + 2\Delta\omega$ respectively. The blue arrows in the top of the figures indicate the later forward and the later time-reversed wave. Clearly, 8a. top (middle and bottom) panel corresponds to (non-)reciprocal response.

43

interface patterned with an array of homogeneous nanostructures that are all modulated similarly in the time domain where $\Delta k_x = 0$ and $\Delta \omega \neq 0$. Equation (4) requires studying both time forward and time backward cases separately. First, we examine the time forward scenario $(t \rightarrow +t)$ where the incident wave is impinging on the metasurface at an angle $\theta_{I,t\rightarrow+t}$ and it is reflected at angle $\theta_{R,t\rightarrow+t}$ calculated given the frequency shift (8c. middle panel left) and given by:

$$\sin \theta_{R,t\rightarrow+t} = \frac{\omega}{\omega + \Delta \omega} \sin \theta_{I,t\rightarrow+t} \tag{7}$$

Now let us suppose the time-reversed scenario $(t \rightarrow -t)$, with an incident wave impinging on the metasurface at an angle $\theta_{I,t\rightarrow-t}$. As shown by the vertical transitions arrows in figure 8b. middle panel (left), in case of time-gradient, the metasurface is modulated so as to add an extra frequency shift $\Delta \omega$ also during the time-reversed process.[214] Such frequency conversions are equivalent to Doppler shifts. Particularly, a Doppler shift can occur when we consider either that the object is moving relatively to the source or similarly that it is stationary but its refractive index varies in time. This frequency conversion is also consistent with energy non-conservation, where a frequency shift is responsible for energy transfer $\Delta E = \hbar \Delta \omega$. We substitute $\frac{\omega}{\omega + \Delta \omega}$ in Eq. (7) with its time-reversed counterpart $\frac{\omega + \Delta \omega}{\omega + 2\Delta \omega}$, leading to a reflected angle $\theta_{R,t\rightarrow-t} \neq \theta_{I,t\rightarrow+t}$. That is, the time modulated metasurface breaks reciprocity. To conserve the initial transverse momentum k_x in the time-reversed case, the presence of the frequency shift modifies the total momentum and the reflected beam direction is thus given by $\sin \theta_{R,t\rightarrow-t} = \frac{k_{\parallel} c}{n(\omega + 2\Delta \omega)}$. The red, green, and blue semicircles in 8c. represent equally spaced frequency curves (isofrequencies) corresponding to frequency values of ω, $\omega + \Delta \omega$ and $\omega + 2\Delta \omega$ respectively, to highlight the change on the length of the total momentum upon temporal modulation.[201]

Space & Time modulated metasurface: for the general case of spatiotemporal mod-

ulation, space and time variations of phase-discontinuities change both the frequency and the tangential momentum of the reflected wave in the time forward scenario $t \rightarrow +t$, as illustrated in figure 8b. and 8c. bottom panels, providing more degrees of freedom in wavefront engineering. One way to achieve spatiotemporal modulation would consist in driving an homogeneous array at a given modulation frequency, making sure that each adjacent pillar is driven with an incremental, but fixed, modulation phase so as to introduce a spatial phase variation at a given time. The time-reversed process shows clearly that the spatiotemporally modulated metasurface breaks reciprocity. The bottom panel in figure 8b. reveals that oblique transitions are needed in (k_x, ω) space to change both the carrier frequency and the wave trajectory in the time-reversed process, leading to $\sin\theta_{R,t\rightarrow -t} = \frac{\omega}{\omega + 2\Delta\omega}\sin\theta_{I,t\rightarrow +t}$. Note that the angle in the time reversed case is not affected by the space gradient, simply because time-reversal symmetry breaking responsible for non-reciprocity is due to the time modulation that changes normal momentum component.[201] In case of fixed phase period and uniform temporal modulation, the spatial variations of the phase discontinuities are thus not affecting the time-reversed process but they can be utilized to address the beam to arbitrary direction in the $t \rightarrow +t$. In the examples provided in figures 8b. and c., non-reciprocal response in the spatial domain requires incoming wave impinging on the metasurface at oblique incidence. However, some cases discussing non-reciprocity upon normal incidence on a time-modulated metasurfaces have been reported.[218,219] Finally, the most general case which could consist in arbitrary temporal modulation of each nano-element taken independently, i.e. not a fixed relative phase between adjacent elements, may provide essentially unlimited wavefront engineering capabilities in both spatial and frequency domains.

Before closing this perspective section, we find it interesting to highlight the difference between metasurfaces which provide asymmetric trajectories as a comparison to metasurfaces presenting non-reciprocal responses. An asymmetric metasurface is a device which deflects light at two different output angles depending on the direction of illumination. This is the case of any basic phase gradient metasurface disposed at an interface between two media,

as it breaks parity-symmetry after inverting the spatial coordinate ($z \to -z$). However, achieving non-reciprocity requires asymmetry upon time reversal.[205] Metasurfaces featuring bianisotropy are in general associated with asymmetric responses. These bianisotropic metasurfaces are dictated by magnetoelectric coupling holding for the excitation of magnetic (electric) dipole moment by electric (magnetic) field leading to anisotropic responses. A solid review highlighting the physics and some interesting aspects of the bianisotropic metasurfaces can be found in.[220] A very characteristic class of bianisotropic metasurfaces encompasses the so-called "chiral" ones. While we often read about planar chiral structures, chirality can only be achieved in the three-dimensional space.[221] Therefore, chiral metasurfaces were mainly proposed as cascaded systems. As an example, we report on a bianisotropic metasurface based on superimposed gold sheets that have demonstrated asymmetric transmission through full polarization control of circularly polarized light. In that case, a Faraday rotation-like behavior has been witnessed, through a magnetic-free approach.[222] Chiral building blocks belong to the so-called reciprocal bianisotropic meta-atoms since no external bias is employed. Interestingly, the bianisotropic coupling has been proposed for engineering non-reciprocal effects relying on the action of external stimuli. Very representative classes of non-reciprocal bianisotropic metasurfaces are the "Tellegen" and the so-called "moving" metasurfaces, generally comprising transitor-loaded structures. Radi et al.[223] proposed a magnet-free Tellegen metasurface that scatters the light asymmetrically when the device is illuminated from different sides.

"Moving" bianisotropic metasurfaces have been also introduced for achieving non-reciprocity. When we are talking about these "moving" metasurfaces we do not mean that our metasurface is in motion. In practice, such metasurfaces may be engineered to incorporate bianisotropy that mimics the behavior of a moving medium.[223,224] In their recent publication, Rad'i and Alu explained that stationary inclusions can be engineered to electromagnetically move towards or against the observer depending on the direction of the observation.[225] They conceptualized a metagrating designed to perform electromagnetic circulation between

three channels. Further perspectives in tunable metasurface-based non-reciprocal devices are expected through the combination of bianisotropy and time-only modulation as has been recently proposed by Wang et al.[226] Such combination may serve at increasing the number of degrees of freedom in designing active non-reciprocal devices by leveraging on bianisotropic properties.[220]

We conclude that the important progress and the advances in the tuning mechanisms reported in this review are promising for fueling the engines to take off the industrial development of metasurfaces. About one decade ago, passive metasurfaces promised and succeeded in revolutionizing our ability to engineer electromagnetic waves, current tunable metasurfaces are bound to play a leading role in the industrialization of disruptive photonic systems. Space &/or time modulation with metasurfaces still have to address several challenges and difficulties. Notably, dedicated research efforts are needed to bring the architectures at optical frequencies, to better integrate and design the electronic drivers, to achieve high efficiency and high modulation performances through optimal design and processes, to develop sophisticated software, and finally to package complex and high density of electronic circuitry on a chip-scale system. Additionally, benchmarking, device testing in real operational conditions and design optimization are also required to demonstrate the reliability of the modulators for applications in AR/VR, LiDARs, and communications. Beyond the huge industrial interest, there is still a lot of space for fundamental research to both tackle existing bottlenecks as well as to foster conceptualization of novel physical phenomena. Particularly, the unexplored field of time-modulated non-reciprocal metasurfaces at optical frequencies is expected to grow significantly in the coming years, offering new application perspectives. Finally, besides the fascinating physical effects and their potential implementation in new optical architectures, simple versions of time-modulated metasurfaces will be utilized to adapt and adjust the optical response of interfaces to operate at various on-demand wavelengths. The road that leads to the realization of an ultimate ultrafast and ultrathin non-reciprocal optical components is certainly challenging but the perspectives of innovation along the road are

extremely exciting. Various approaches considered in this manuscript have the potential to impact the field of photonics in both academic and industrial sectors, offering researchers working in this area an unlimited source of inspiration and innovations.

Acknowledgement

Funding sources

References

(1) Genevet, P.; Capasso, F.; Aieta, F.; Khorasaninejad, M.; Devlin, R. Recent advances in planar optics: from plasmonic to dielectric metasurfaces. Optica **2017**, 4, 139–152.

(2) Chen, H.-T.; Taylor, A. J.; Yu, N. A review of metasurfaces: physics and applications. Reports on Progress in Physics **2016**, 79.

(3) Scheuer, J. Optical Metasurfaces Are Coming of Age: Short- and Long-Term Opportunities for Commercial Applications. ACS Photonics **2020**, 7, 1323–1354, Publisher: American Chemical Society.

(4) Sun, S.; He, Q.; Xiao, S.; Xu, Q.; Li, X.; Zhou, L. Gradient-index meta-surfaces as a bridge linking propagating waves and surface waves. Nature Materials **2012**, 11.

(5) Grady, N. K.; Heyes, J. E.; Chowdhury, D. R.; Zeng, Y.; Reiten, M. T.; Azad, A. K.; Taylor, A. J.; Dalvit, D. A. R.; Chen, H.-T. Terahertz Metamaterials for Linear Polarization Conversion and Anomalous Refraction. Science **2013**, 340.

(6) Song, Q.; Khadir, S.; Vézian, S.; Damilano, B.; Mierry, P. D.; Chenot, S.; Brandli, V.; Genevet, P. Bandwidth-unlimited polarization-maintaining metasurfaces. Science Advances **2021**, 7.

(7) Sawant, R.; Andrén, D.; Martins, R. J.; Khadir, S.; Verre, R.; Käll, M.; Genevet, P. Aberration-corrected large-scale hybrid metalenses. Optica **2021**, 8, 1405–1411.

(8) Song, Q.; Baroni, A.; Wu, P. C.; Chenot, S.; Brandli, V.; Vézian, S.; Damilano, B.; de Mierry, P.; Khadir, S.; Ferrand, P.; Genevet, P. Broadband decoupling of intensity and polarization with vectorial Fourier metasurfaces. Nature Communications **2021**, 12.

(9) Ren, H.; Briere, G.; Fang, X.; Ni, P.; Sawant, R.; Héron, S.; Chenot, S.; Vézian, S.; Damilano, B.; Brändli, V.; Maier, S. A.; Genevet, P. Metasurface orbital angular momentum holography. Nature Communications **2019**, 10.

(10) Zhang, L.; Chen, X. Q.; Liu, S.; Zhang, Q.; Zhao, J.; Dai, J. Y.; Bai, G. D.; Wan, X.; Cheng, Q.; Castaldi, G.; Galdi, V.; Cui, T. J. Space-time-coding digital metasurfaces. Nature Communications **2018**, 9.

(11) Miroshnichenko, A. E.; Kivshar, Y. S. Polarization Traffic Control for Surface Plasmons. Science **2013**, 340.

(12) Arbabi, A.; Horie, Y.; Bagheri, M.; Faraon, A. Dielectric metasurfaces for complete

control of phase and polarization with subwavelength spatial resolution and high transmission. Nature Nanotechnology **2015**, _10_.

(13) Dorrah, A. H.; Rubin, N. A.; Zaidi, A.; Tamagnone, M.; Capasso, F. Metasurface optics for on-demand polarization transformations along the optical path. Nature Photonics **2021**, _15_.

(14) Leitis, A.; Tseng, M. L.; John-Herpin, A.; Kivshar, Y. S.; Altug, H. Wafer-Scale Functional Metasurfaces for Mid-Infrared Photonics and Biosensing. Advanced Materials **2021**, _33_, 2102232.

(15) Luo, X.; Hu, Y.; Li, X.; Jiang, Y.; Wang, Y.; Dai, P.; Liu, Q.; Shu, Z.; Duan, H. Integrated Metasurfaces with Microprints and Helicity-Multiplexed Holograms for Real-Time Optical Encryption. Advanced Optical Materials **2020**, _8_, 1902020.

(16) Kwon, H.; Arbabi, E.; Kamali, S. M.; Faraji-Dana, M.; Faraon, A. Single-shot quantitative phase gradient microscopy using a system of multifunctional metasurfaces. Nature Photonics **2020**, _14_, 109–114.

(17) Yu, N.; Genevet, P.; Kats, M. A.; Aieta, F.; Tetienne, J.-P.; Capasso, F.; Gaburro, Z. Light Propagation with Phase Discontinuities: Generalized Laws of Reflection and Refraction. Science **2011**, _334_, 333–337.

(18) Lalanne, P.; Astilean, S.; Chavel, P.; Cambril, E.; Launois, H. Blazed binary subwavelength gratings with efficiencies larger than those of conventional échelette gratings. Optics Letters **1998**, _23_.

(19) Berry, M. The Adiabatic Phase and Pancharatnam's Phase for Polarized Light. Journal of Modern Optics **1987**, _34_.

(20) Biener, G.; Niv, A.; Kleiner, V.; Hasman, E. Formation of helical beams by use of Pancharatnam–Berry phase optical elements. Optics Letters **2002**, _27_.

(21) Song, Q.; Odeh, M.; Zúñiga-Pérez, J.; Kanté, B.; Genevet, P. Plasmonic topological metasurface by encircling an exceptional point. Science **2021**, 373, 1133–1137.

(22) Kwon, H.; Sounas, D.; Cordaro, A.; Polman, A.; Alù, A. Nonlocal metasurfaces for optical signal processing. Physical review letters **2018**, 121, 173004.

(23) Malek, S. C.; Overvig, A. C.; Alù, A.; Yu, N. Resonant wavefront-shaping flat optics. arXiv preprint arXiv:2009.07054 **2020**,

(24) Malek, S. C.; Overvig, A. C.; Shrestha, S.; Yu, N. Active nonlocal metasurfaces. Nanophotonics **2021**, 10, 655–665.

(25) Song, J. H.; van de Groep, J.; Kim, S. J.; Brongersma, M. L. Nonlocal metasurfaces for spectrally decoupled wavefront manipulation and eye tracking. ArXiv **2021**, abs/2102.05790.

(26) Xie, Y.-Y.; Ni, P.-N.; Wang, Q.-H.; Kan, Q.; Briere, G.; Chen, P.-P.; Zhao, Z.-Z.; Delga, A.; Ren, H.-R.; Chen, H.-D.; Xu, C.; Genevet, P. Metasurface-integrated vertical cavity surface-emitting lasers for programmable directional lasing emissions. Nature Nanotechnology **2020**, 15.

(27) Wang, Q.-H.; Ni, P.-N.; Xie, Y.-Y.; Kan, Q.; Chen, P.-P.; Fu, P.; Deng, J.; Jin, T.-L.; Chen, H.-D.; Lee, H. W. H.; Xu, C.; Genevet, P. On-Chip Generation of Structured Light Based on Metasurface Optoelectronic Integration. Laser & Photonics Reviews **2021**, 15.

(28) Arbabi, E.; Kamali, S. M.; Arbabi, A.; Faraon, A. Full-Stokes Imaging Polarimetry Using Dielectric Metasurfaces. ACS Photonics **2018**, 5, 3132–3140.

(29) Mueller, J. P. B.; Leosson, K.; Capasso, F. Ultracompact metasurface in-line polarimeter. Optica **2016**, 3, 42–47.

(30) Sievenpiper, D.; Schaffner, J.; Song, H.; Loo, R.; Tangonan, G. Two-dimensional beam steering using an electrically tunable impedance surface. <u>IEEE Transactions on Antennas and Propagation</u> **2003**, <u>51</u>.

(31) Cui, T. J.; Qi, M. Q.; Wan, X.; Zhao, J.; Cheng, Q. Coding metamaterials, digital metamaterials and programmable metamaterials. <u>Light: Science & Applications</u> **2014**, <u>3</u>.

(32) Watts, C. M.; Shrekenhamer, D.; Montoya, J.; Lipworth, G.; Hunt, J.; Sleasman, T.; Krishna, S.; Smith, D. R.; Padilla, W. J. Terahertz compressive imaging with metamaterial spatial light modulators. <u>Nature Photonics</u> **2014**, <u>8</u>, 605–609.

(33) Zhu, W. et al. A Flat Lens with Tunable Phase Gradient by Using Random Access Reconfigurable Metamaterial. <u>Advanced Materials</u> **2015**, <u>27</u>, 4739–4743.

(34) Xu, H.-X.; Sun, S.; Tang, S.; Ma, S.; He, Q.; Wang, G.-M.; Cai, T.; Li, H.-P.; Zhou, L. Dynamical control on helicity of electromagnetic waves by tunable metasurfaces. <u>Scientific Reports</u> **2016**, <u>6</u>.

(35) Li, L.; Jun Cui, T.; Ji, W.; Liu, S.; Ding, J.; Wan, X.; Bo Li, Y.; Jiang, M.; Qiu, C.-W.; Zhang, S. Electromagnetic reprogrammable coding-metasurface holograms. <u>Nature Communications</u> **2017**, <u>8</u>.

(36) Chen, K.; Feng, Y.; Monticone, F.; Zhao, J.; Zhu, B.; Jiang, T.; Zhang, L.; Kim, Y.; Ding, X.; Zhang, S.; Alù, A.; Qiu, C.-W. A Reconfigurable Active Huygens' Metalens. <u>Advanced Materials</u> **2017**, <u>29</u>.

(37) Shao, L.; Zhu, W. Electrically Reconfigurable Microwave Metasurfaces With Active Lumped Elements: A Mini Review. <u>Frontiers in Materials</u> **2021**, <u>8</u>, 689665.

(38) Bang, S.; Kim, J.; Yoon, G.; Tanaka, T.; Rho, J. Recent Advances in Tunable and Reconfigurable Metamaterials. <u>Micromachines</u> **2018**, <u>9</u>, 560.

(39) He, Q.; Sun, S.; Zhou, L. Tunable/Reconfigurable Metasurfaces: Physics and Applications. Research **2019**, 1–16.

(40) Nemati, A.; Wang, Q.; Hong, M.; Teng, J. Tunable and reconfigurable metasurfaces and metadevices. Opto-Electronic Advances **2018**, 1.

(41) Lee, C.-W.; Choi, H. J.; Jeong, H. Tunable metasurfaces for visible and SWIR applications. Nano Convergence **2020**, 7, 3.

(42) Shalaginov, M. Y.; Campbell, S. D.; An, S.; Zhang, Y.; Ríos, C.; Whiting, E. B.; Wu, Y.; Kang, L.; Zheng, B.; Fowler, C.; Zhang, H.; Werner, D. H.; Hu, J.; Gu, T. Design for quality: reconfigurable flat optics based on active metasurfaces. Nanophotonics **2020**, 9, 3505–3534.

(43) Shaltout, A. M.; Shalaev, V. M.; Brongersma, M. L. Spatiotemporal light control with active metasurfaces. Science **2019**, 364.

(44) Kang, L.; Jenkins, R. P.; Werner, D. H. Recent Progress in Active Optical Metasurfaces. Advanced Optical Materials **2019**, 7, 1801813.

(45) Kim, I.; Martins, R. J.; Jang, J.; Badloe, T.; Khadir, S.; Jung, H.-Y.; Kim, H.; Kim, J.; Genevet, P.; Rho, J. Nanophotonics for light detection and ranging technology. Nature Nanotechnology **2021**, 16.

(46) Zhou, T.; Lin, X.; Wu, J.; Chen, Y.; Xie, H.; Li, Y.; Fan, J.; Wu, H.; Fang, L.; Dai, Q. Large-scale neuromorphic optoelectronic computing with a reconfigurable diffractive processing unit. Nature Photonics **2021**, 15, 367–373.

(47) Wuttig, M.; Bhaskaran, H.; Taubner, T. Phase-change materials for non-volatile photonic applications. Nature Photonics **2017**, 11.

(48) Abdollahramezani, S.; Hemmatyar, O.; Taghinejad, H.; Krasnok, A.; Kiarashine-jad, Y.; Zandehshahvar, M.; Alù, A.; Adibi, A. Tunable nanophotonics enabled by chalcogenide phase-change materials. Nanophotonics **2020**, 9, 1189–1241.

(49) Ke, Y.; Wang, S.; Liu, G.; Li, M.; White, T. J.; Long, Y. Vanadium dioxide: The multistimuli responsive material and its applications. Small **2018**, 14, 1802025.

(50) Cueff, S.; John, J.; Zhang, Z.; Parra, J.; Sun, J.; Orobtchouk, R.; Ramanathan, S.; Sanchis, P. VO2 nanophotonics. APL Photonics **2020**, 5, 110901.

(51) Ding, F.; Yang, Y.; Bozhevolnyi, S. I. Dynamic Metasurfaces Using Phase-Change Chalcogenides. Advanced Optical Materials **2019**, 7.

(52) Meng, Y.; Cao, T.; Long, Y. Progress in metasurfaces based on Ge–Sb–Te phase-change materials. Journal of Applied Physics **2020**, 128, 140904.

(53) Zhang, Y.; Ríos, C.; Shalaginov, M. Y.; Li, M.; Majumdar, A.; Gu, T.; Hu, J. Myths and truths about optical phase change materials: A perspective. Applied Physics Letters **2021**, 118, 210501.

(54) Cueff, S.; Taute, A.; Bourgade, A.; Lumeau, J.; Monfray, S.; Song, Q.; Genevet, P.; Devif, B.; Letartre, X.; Berguiga, L. Reconfigurable Flat Optics with Programmable Reflection Amplitude Using Lithography-Free Phase-Change Material Ultra-Thin Films. Advanced Optical Materials **2021**, 9.

(55) Wan, C.; Zhang, Z.; Woolf, D.; Hessel, C. M.; Rensberg, J.; Hensley, J. M.; Xiao, Y.; Shahsafi, A.; Salman, J.; Richter, S., et al. On the optical properties of thin-film vanadium dioxide from the visible to the far infrared. Annalen der Physik **2019**, 531, 1900188.

(56) Zhang, Y. et al. Electrically reconfigurable non-volatile metasurface using low-loss optical phase-change material. Nature Nanotechnology **2021**, 16, 661–666.

(57) Teo, T. Y.; Krbal, M.; Mistrik, J.; Prikryl, J.; Lu, L.; Simpson, R. E. Comparison and analysis of phase change materials-based reconfigurable silicon photonic directional couplers. Optical Materials Express **2022**, 12, 606–621.

(58) Lawson, D.; Hewak, D. W.; Muskens, O. L.; Zeimpekis, I. Time-resolved reversible optical switching of the ultralow-loss phase change material Sb2Se3. arXiv preprint arXiv:2111.13182 **2021**,

(59) Zhang, H.; Yang, X.; Chen, J.; Rahman, B.; Zhou, L., et al. Comparison of the phase change process in a GST-loaded silicon waveguide and MMI. Optics Express **2021**, 29, 3503–3514.

(60) Delaney, M.; Zeimpekis, I.; Lawson, D.; Hewak, D. W.; Muskens, O. L. A New Family of Ultralow Loss Reversible Phase-Change Materials for Photonic Integrated Circuits: Sb2S3 and Sb2Se3. Advanced Functional Materials **2020**, 30.

(61) Dong, W.; Liu, H.; Behera, J. K.; Lu, L.; Ng, R. J.; Sreekanth, K. V.; Zhou, X.; Yang, J. K.; Simpson, R. E. Wide bandgap phase change material tuned visible photonics. Advanced Functional Materials **2019**, 29.

(62) Zhang, Y.; Chou, J. B.; Li, J.; Li, H.; Du, Q.; Yadav, A.; Zhou, S.; Shalaginov, M. Y.; Fang, Z.; Zhong, H., et al. Broadband transparent optical phase change materials for high-performance nonvolatile photonics. Nature communications **2019**, 10, 1–9.

(63) Imada, M.; Fujimori, A.; Tokura, Y. Metal-insulator transitions. Reviews of modern physics **1998**, 70, 1039.

(64) Cavalleri, A.; Tóth, C.; Siders, C. W.; Squier, J.; Ráksi, F.; Forget, P.; Kieffer, J. Femtosecond structural dynamics in VO 2 during an ultrafast solid-solid phase transition. Physical review letters **2001**, 87, 237401.

(65) Jeong, Y.; Bahk, Y.; Kim, D. Dynamic Terahertz Plasmonics Enabled by Phase-Change Materials. Advanced Optical Materials **2020**, 8, 1900548.

(66) Shabanpour, J.; Beyraghi, S.; Cheldavi, A. Ultrafast reprogrammable multifunctional vanadium-dioxide-assisted metasurface for dynamic THz wavefront engineering. Scientific Reports **2020**, 10, 8950.

(67) Rini, M.; Cavalleri, A.; Schoenlein, R. W.; López, R.; Feldman, L. C.; Haglund, R. F.; Boatner, L. A.; Haynes, T. E. Photoinduced phase transition in VO 2 nanocrystals: ultrafast control of surface-plasmon resonance. Optics letters **2005**, 30, 558–560.

(68) Cueff, S.; Li, D.; Zhou, Y.; Wong, F. J.; Kurvits, J. A.; Ramanathan, S.; Zia, R. Dynamic control of light emission faster than the lifetime limit using VO 2 phase-change. Nature communications **2015**, 6, 1–6.

(69) John, J.; Gutierrez, Y.; Zhang, Z.; Karl, H.; Ramanathan, S.; Orobtchouk, R.; Moreno, F.; Cueff, S. Multipolar resonances with designer tunability using VO 2 phase-change materials. Physical Review Applied **2020**, 13, 044053.

(70) Howes, A.; Zhu, Z.; Curie, D.; Avila, J. R.; Wheeler, V. D.; Haglund, R. F.; Valentine, J. G. Optical Limiting Based on Huygens' Metasurfaces. Nano Letters **2020**, 20, 4638–4644.

(71) Kepic, P.; Ligmajer, F.; Hrton, M.; Ren, H.; Menezes, L. d. S.; Maier, S. A.; Sikola, T. Optically Tunable Mie Resonance VO2 Nanoantennas for Metasurfaces in the Visible. ACS Photonics **2021**, 8, 1048–1057.

(72) Tripathi, A.; John, J.; Kruk, S.; Zhang, Z.; Nguyen, H. S.; Berguiga, L.; Romeo, P. R.; Orobtchouk, R.; Ramanathan, S.; Kivshar, Y., et al. Tunable Mie-Resonant Dielectric Metasurfaces Based on VO2 Phase-Transition Materials. ACS Photonics **2021**, 8, 1206–1213.

(73) Zhu, Z.; Evans, P. G.; Haglund Jr, R. F.; Valentine, J. G. Dynamically reconfigurable metadevice employing nanostructured phase-change materials. Nano letters **2017**, 17, 4881–4885.

(74) Kim, Y.; Wu, P. C.; Sokhoyan, R.; Mauser, K.; Glaudell, R.; Kafaie Shirmanesh, G.; Atwater, H. A. Phase modulation with electrically tunable vanadium dioxide phase-change metasurfaces. Nano letters **2019**, 19, 3961–3968.

(75) Butakov, N. A.; Knight, M. W.; Lewi, T.; Iyer, P. P.; Higgs, D.; Chorsi, H. T.; Trastoy, J.; Del Valle Granda, J.; Valmianski, I.; Urban, C.; Kalcheim, Y.; Wang, P. Y.; Hon, P. W. C.; Schuller, I. K.; Schuller, J. A. Broadband Electrically Tunable Dielectric Resonators Using Metal–Insulator Transitions. ACS Photonics **2018**, 5, 4056–4060.

(76) Liu, Z.; Banar, B.; Butun, S.; Kocer, H.; Wang, K.; Scheuer, J.; Wu, J.; Aydin, K. Dynamic infrared thin-film absorbers with tunable absorption level based on VO $_2$ phase transition. Optical Materials Express **2018**, 8, 2151.

(77) Dong, K.; Hong, S.; Deng, Y.; Ma, H.; Li, J.; Wang, X.; Yeo, J.; Wang, L.; Lou, S.; Tom, K. B., et al. A Lithography-Free and Field-Programmable Photonic Metacanvas. Advanced Materials **2018**, 30, 1703878.

(78) Liu, L.; Kang, L.; Mayer, T. S.; Werner, D. H. Hybrid metamaterials for electrically triggered multifunctional control. Nature communications **2016**, 7, 1–8.

(79) Cai, H.; Chen, S.; Zou, C.; Huang, Q.; Liu, Y.; Hu, X.; Fu, Z.; Zhao, Y.; He, H.; Lu, Y. Multifunctional hybrid metasurfaces for dynamic tuning of terahertz waves. Advanced Optical Materials **2018**, 6, 1800257.

(80) Wuttig, M.; Deringer, V. L.; Gonze, X.; Bichara, C.; Raty, J.-Y. Incipient metals: functional materials with a unique bonding mechanism. Advanced materials **2018**, 30, 1803777.

(81) Kooi, B. J.; Wuttig, M. Chalcogenides by design: Functionality through metavalent bonding and confinement. Advanced Materials **2020**, 32.

(82) Raeis-Hosseini, N.; Rho, J. Metasurfaces Based on Phase-Change Material as a Reconfigurable Platform for Multifunctional Devices. Materials **2017**, 10, 1046.

(83) Yang, H.; Xie, Z.; He, H.; Zhang, Q.; Li, J.; Zhang, Y.; Yuan, X. Switchable imaging between edge-enhanced and bright-field based on a phase-change metasurface. Optics Letters **2021**, 46, 3741–3744.

(84) Yin, X.; Steinle, T.; Huang, L.; Taubner, T.; Wuttig, M.; Zentgraf, T.; Giessen, H. Beam switching and bifocal zoom lensing using active plasmonic metasurfaces. Light: Science & Applications **2017**, 6.

(85) Tittl, A.; Michel, A.-K. U.; Schäferling, M.; Yin, X.; Gholipour, B.; Cui, L.; Wuttig, M.; Taubner, T.; Neubrech, F.; Giessen, H. A Switchable Mid-Infrared Plasmonic Perfect Absorber with Multispectral Thermal Imaging Capability. Advanced Materials **2015**, 27.

(86) Wang, Q.; Rogers, E. T. F.; Gholipour, B.; Wang, C.-M.; Yuan, G.; Teng, J.; Zheludev, N. I. Optically reconfigurable metasurfaces and photonic devices based on phase change materials. Nature Photonics **2016**, 10, 60–65.

(87) Li, P.; Yang, X.; Maß, T. W. W.; Hanss, J.; Lewin, M.; Michel, A.-K. U.; Wuttig, M.; Taubner, T. Reversible optical switching of highly confined phonon–polaritons with an ultrathin phase-change material. Nature Materials **2016**, 15, 870–875.

(88) Raoux, S.; Xiong, F.; Wuttig, M.; Pop, E. Phase change materials and phase change memory. MRS Bulletin **2014**, 39, 703–710.

(89) Cappelletti, P.; Annunziata, R.; Arnaud, F.; Disegni, F.; Maurelli, A.; Zuliani, P.

Phase change memory for automotive grade embedded NVM applications. Journal of Physics D: Applied Physics **2020**, 53, 193002.

(90) Wang, Y.; Landreman, P.; Schoen, D.; Okabe, K.; Marshall, A.; Celano, U.; Wong, H.-S. P.; Park, J.; Brongersma, M. L. Electrical tuning of phase-change antennas and metasurfaces. Nature Nanotechnology **2021**, 16, 667–672.

(91) Zheng, J.; Fang, Z.; Wu, C.; Zhu, S.; Xu, P.; Doylend, J. K.; Deshmukh, S.; Pop, E.; Dunham, S.; Li, M.; Majumdar, A. Nonvolatile Electrically Reconfigurable Integrated Photonic Switch Enabled by a Silicon PIN Diode Heater. Advanced Materials **2020**, 32, 2001218.

(92) Lepeshov, S.; Krasnok, A. Tunable phase-change metasurfaces. Nature Nanotechnology **2021**, 16, 615–616.

(93) Abdollahramezani, S.; Hemmatyar, O.; Taghinejad, M.; Taghinejad, H.; Krasnok, A.; Eftekhar, A. A.; Teichrib, C.; Deshmukh, S.; El-Sayed, M.; Pop, E., et al. Electrically driven programmable phase-change meta-switch reaching 80% efficiency. arXiv preprint arXiv:2104.10381 **2021**,

(94) Alvarez-Alegria, M.; Siegel, J.; Garcia-Pardo, M.; Cabello, F.; Toudert, J.; Haro-Poniatowski, E.; Serna, R. Nanosecond Laser Switching of Phase-Change Random Metasurfaces with Tunable ON-State. Advanced Optical Materials **2021**, 2101405.

(95) Fang, Z.; Zheng, J.; Saxena, A.; Whitehead, J.; Chen, Y.; Majumdar, A. Non-Volatile Reconfigurable Integrated Photonics Enabled by Broadband Low-Loss Phase Change Material. Advanced Optical Materials **2021**, 9.

(96) Hemmatyar, O.; Abdollahramezani, S.; Zeimpekis, I.; Lepeshov, S.; Krasnok, A.; Khan, A. I.; Neilson, K. M.; Teichrib, C.; Brown, T.; Pop, E.; Hewak, D. W.; Wuttig, M.; Alu, A.; Muskens, O. L.; Adibi, A. Enhanced Meta-Displays Using Advanced Phase-Change Materials. arXiv:2107.12159 [physics] **2021**, arXiv: 2107.12159.

(97) Michel, A.-K. U.; Heßler, A.; Meyer, S.; Pries, J.; Yu, Y.; Kalix, T.; Lewin, M.; Hanss, J.; De Rose, A.; Maß, T. W., et al. Advanced Optical Programming of Individual Meta-Atoms Beyond the Effective Medium Approach. Advanced Materials **2019**, 31, 1901033.

(98) Arnaud, F.; Zuliani, P.; Reynard, J.; Gandolfo, A.; Disegni, F.; Mattavelli, P.; Gomiero, E.; Samanni, G.; Jahan, C.; Berthelon, R., et al. Truly innovative 28nm FD-SOI technology for automotive micro-controller applications embedding 16MB phase change memory. 2018 IEEE International Electron Devices Meeting (IEDM). 2018; pp 18–4.

(99) Yu, S.; Wu, X.; Wang, Y.; Guo, X.; Tong, L. 2D Materials for Optical Modulation: Challenges and Opportunities. Advanced Materials **2017**, 29, 1606128.

(100) Ren, F.; Li, M.; Gao, Q.; Cowell, W.; Luo, J.; Jen, A. K.-Y.; Wang, A. X. Surface-normal plasmonic modulator using sub-wavelength metal grating on electro-optic polymer thin film. Optics Communications **2015**, 352, 116–120.

(101) Zhang, J.; Kosugi, Y.; Otomo, A.; Ho, Y.-L.; Delaunay, J.-J.; Nakano, Y.; Tanemura, T. Electrical tuning of metal-insulator-metal metasurface with electro-optic polymer. Applied Physics Letters **2018**, 113, 231102.

(102) Karvounis, A.; Vogler-Neuling, V. V.; Richter, F. U.; Dénervaud, E.; Timofeeva, M.; Grange, R. Electro-Optic Metasurfaces Based on Barium Titanate Nanoparticle Films. Advanced Optical Materials **2020**, 8.

(103) Weigand, H.; Vogler-Neuling, V. V.; Escalé, M. R.; Pohl, D.; Richter, F. U.; Karvounis, A.; Timpu, F.; Grange, R. Enhanced Electro-Optic Modulation in Resonant Metasurfaces of Lithium Niobate. ACS Photonics **2021**, 8, 3004–3009, Publisher: American Chemical Society.

(104) Gao, B.; Ren, M.; Wu, W.; Cai, W.; Xu, J. Electro-Optic Lithium Niobate Metasurfaces. arXiv:2101.06491 [physics] **2021**,

(105) Benea-Chelmus, I.-C.; Mason, S.; Meretska, M. L.; Elder, D. L.; Kazakov, D.; Shams-Ansari, A.; Dalton, L. R.; Capasso, F. Gigahertz free-space electro-optic modulators based on Mie resonances. 2021.

(106) Kuo, Y.-H.; Lee, Y. K.; Ge, Y.; Ren, S.; Roth, J. E.; Kamins, T. I.; Miller, D. A. B.; Harris, J. S. Strong quantum-confined Stark effect in germanium quantum-well structures on silicon. Nature **2005**, 437, 1334–1336.

(107) Wu, P. C.; Pala, R. A.; Kafaie Shirmanesh, G.; Cheng, W.-H.; Sokhoyan, R.; Grajower, M.; Alam, M. Z.; Lee, D.; Atwater, H. A. Dynamic beam steering with all-dielectric electro-optic III–V multiple-quantum-well metasurfaces. Nature Communications **2019**, 10, 3654.

(108) Lee, J.; Jung, S.; Chen, P.-Y.; Lu, F.; Demmerle, F.; Boehm, G.; Amann, M.-C.; Alù, A.; Belkin, M. A. Ultrafast Electrically Tunable Polaritonic Metasurfaces. Advanced Optical Materials **2014**, 2, 1057–1063.

(109) Monat, C.; Su, Y. Hybrid photonics beyond silicon. APL Photonics **2020**, 5, 020402.

(110) Zhu, D.; Shao, L.; Yu, M.; Cheng, R.; Desiatov, B.; Xin, C. J.; Hu, Y.; Holzgrafe, J.; Ghosh, S.; Shams-Ansari, A.; Puma, E.; Sinclair, N.; Reimer, C.; Zhang, M.; Lončar, M. Integrated photonics on thin-film lithium niobate. Advances in Optics and Photonics **2021**, 13, 242.

(111) Elshaari, A. W.; Pernice, W.; Srinivasan, K.; Benson, O.; Zwiller, V. Hybrid integrated quantum photonic circuits. Nature Photonics **2020**, 14.

(112) Olivieri, A.; Chen, C.; Hassan, S.; Lisicka-Skrzek, E.; Tait, R. N.; Berini, P. Plasmonic

Nanostructured Metal–Oxide–Semiconductor Reflection Modulators. Nano Letters **2015**, 15, 2304–2311.

(113) Iyer, P. P.; Pendharkar, M.; Schuller, J. A. Electrically Reconfigurable Metasurfaces Using Heterojunction Resonators. Advanced Optical Materials **2016**, 4, 1582–1588.

(114) Liu, X.; Kang, J.-H.; Yuan, H.; Park, J.; Cui, Y.; Hwang, H. Y.; Brongersma, M. L. Tuning of Plasmons in Transparent Conductive Oxides by Carrier Accumulation. ACS Photonics **2018**, 5, 1493–1498.

(115) Anopchenko, A.; Tao, L.; Arndt, C.; Lee, H. W. H. Field-Effect Tunable and Broadband Epsilon-Near-Zero Perfect Absorbers with Deep Subwavelength Thickness. ACS Photonics **2018**, 5, 2631–2637.

(116) Howes, A.; Wang, W.; Kravchenko, I.; Valentine, J. Dynamic transmission control based on all-dielectric Huygens metasurfaces. Optica **2018**, 5, 787.

(117) Alam, M. Z.; Schulz, S. A.; Upham, J.; De Leon, I.; Boyd, R. W. Large optical non-linearity of nanoantennas coupled to an epsilon-near-zero material. Nature Photonics **2018**, 12.

(118) Kafaie Shirmanesh, G.; Sokhoyan, R.; Pala, R. A.; Atwater, H. A. Dual-Gated Active Metasurface at 1550 nm with Wide (>300°) Phase Tunability. Nano Letters **2018**, 18, 2957–2963.

(119) Forouzmand, A.; Salary, M. M.; Inampudi, S.; Mosallaei, H. A Tunable Multigate Indium-Tin-Oxide-Assisted All-Dielectric Metasurface. Advanced Optical Materials **2018**, 6, 1701275.

(120) Forouzmand, A.; Mosallaei, H. Electro-optical Amplitude and Phase Modulators Based on Tunable Guided-Mode Resonance Effect. ACS Photonics **2019**, 6, 2860–2869.

(121) Lee, Y.; Yun, J.; Kim, S.; Seo, M.; In, S.; Jeong, H.; Lee, S.; Park, N.; Chung, T. D.; Lee, B. High-Speed Transmission Control in Gate-Tunable Metasurfaces Using Hybrid Plasmonic Waveguide Mode. Advanced Optical Materials **2020**, 8, 2001256.

(122) Shirmanesh, G. K.; Sokhoyan, R.; Wu, P. C.; Atwater, H. A. Electro-optically Tunable Multifunctional Metasurfaces. ACS Nano **2020**, 14, 6912–6920.

(123) Morea, M.; Zang, K.; Kamins, T. I.; Brongersma, M. L.; Harris, J. S. Electrically Tunable, CMOS-Compatible Metamaterial Based on Semiconductor Nanopillars. ACS Photonics **2018**, 5, 4702–4709.

(124) Yan, H.; Low, T.; Zhu, W.; Wu, Y.; Freitag, M.; Li, X.; Guinea, F.; Avouris, P.; Xia, F. Damping pathways of mid-infrared plasmons in graphene nanostructures. Nature Photonics **2013**, 7, 394–399.

(125) Brar, V. W.; Jang, M. S.; Sherrott, M.; Lopez, J. J.; Atwater, H. A. Highly Confined Tunable Mid-Infrared Plasmonics in Graphene Nanoresonators. Nano Letters **2013**, 13, 2541–2547.

(126) Yao, Y.; Kats, M. A.; Genevet, P.; Yu, N.; Song, Y.; Kong, J.; Capasso, F. Broad Electrical Tuning of Graphene-Loaded Plasmonic Antennas. Nano Letters **2013**, 13, 1257–1264.

(127) Kim, T.-T.; Oh, S. S.; Kim, H.-D.; Park, H. S.; Hess, O.; Min, B.; Zhang, S. Electrical access to critical coupling of circularly polarized waves in graphene chiral metamaterials. Science Advances **2017**, 3.

(128) Huang, Z.; Yao, K.; Su, G.; Ma, W.; Li, L.; Liu, Y.; Zhan, P.; Wang, Z. Graphene–metal hybrid metamaterials for strong and tunable circular dichroism generation. Optics Letters **2018**, 43, 2636.

(129) Biswas, S. R.; Gutiérrez, C. E.; Nemilentsau, A.; Lee, I.-H.; Oh, S.-H.; Avouris, P.; Low, T. Tunable Graphene Metasurface Reflectarray for Cloaking, Illusion, and Focusing. Physical Review Applied **2018**, 9, 034021.

(130) Han, S.; Kim, S.; Kim, S.; Low, T.; Brar, V. W.; Jang, M. S. Complete Complex Amplitude Modulation with Electronically Tunable Graphene Plasmonic Metamolecules. ACS Nano **2020**, 14, 1166–1175.

(131) Sherrott, M. C.; Hon, P. W. C.; Fountaine, K. T.; Garcia, J. C.; Ponti, S. M.; Brar, V. W.; Sweatlock, L. A.; Atwater, H. A. Experimental Demonstration of >230° Phase Modulation in Gate-Tunable Graphene–Gold Reconfigurable Mid-Infrared Metasurfaces. Nano Letters **2017**, 17, 3027–3034, Publisher: American Chemical Society.

(132) Kim, S.; Jang, M. S.; Brar, V. W.; Mauser, K. W.; Kim, L.; Atwater, H. A. Electronically Tunable Perfect Absorption in Graphene. Nano Letters **2018**, 18, 971–979.

(133) Lee, H. W.; Papadakis, G.; Burgos, S. P.; Chander, K.; Kriesch, A.; Pala, R.; Peschel, U.; Atwater, H. A. Nanoscale Conducting Oxide PlasMOStor. Nano Letters **2014**, 14, 6463–6468.

(134) Park, J. et al. All-solid-state spatial light modulator with independent phase and amplitude control for three-dimensional LiDAR applications. Nature Nanotechnology **2021**, 16, 69–76.

(135) Davis, J.; Hsieh, Y.-H.; Lee, H.-C. Humans perceive flicker artifacts at 500 Hz. Scientific Reports **2015**, 5, 7861.

(136) Yu, P.; Li, J.; Zhang, S.; Jin, Z.; Schütz, G.; Qiu, C.-W.; Hirscher, M.; Liu, N. Dynamic Janus Metasurfaces in the Visible Spectral Region. Nano Letters **2018**, 18, 4584–4589.

(137) Li, J.; Kamin, S.; Zheng, G.; Neubrech, F.; Zhang, S.; Liu, N. Addressable metasurfaces for dynamic holography and optical information encryption. Science Advances **2018**, 4.

(138) Yu, P.; Li, J.; Li, X.; Schütz, G.; Hirscher, M.; Zhang, S.; Liu, N. Generation of Switchable Singular Beams with Dynamic Metasurfaces. ACS Nano **2019**, 13, 7100–7106.

(139) Xu, T.; Walter, E. C.; Agrawal, A.; Bohn, C.; Velmurugan, J.; Zhu, W.; Lezec, H. J.; Talin, A. A. High-contrast and fast electrochromic switching enabled by plasmonics. Nature Communications **2016**, 7, 10479.

(140) Peng, J.; Jeong, H.-H.; Lin, Q.; Cormier, S.; Liang, H.-L.; De Volder, M. F.; Vignolini, S.; Baumberg, J. J. Scalable electrochromic nanopixels using plasmonics. Science advances **2019**, 5, eaaw2205.

(141) Kaissner, R.; Li, J.; Lu, W.; Li, X.; Neubrech, F.; Wang, J.; Liu, N. Electrochemically controlled metasurfaces with high-contrast switching at visible frequencies. Science Advances **2021**, 7.

(142) Chen, S.; Kang, E. S. H.; Shiran Chaharsoughi, M.; Stanishev, V.; Kühne, P.; Sun, H.; Wang, C.; Fahlman, M.; Fabiano, S.; Darakchieva, V.; Jonsson, M. P. Conductive polymer nanoantennas for dynamic organic plasmonics. Nature Nanotechnology **2020**, 15, 35–40.

(143) Xiao, L.; Lv, Y.; Lin, J.; Hu, Y.; Dong, W.; Guo, X.; Fan, Y.; Zhang, N.; Zhao, J.; Wang, Y.; Liu, X. WO $_3$ -Based Electrochromic Distributed Bragg Reflector: Toward Electrically Tunable Microcavity Luminescent Device. Advanced Optical Materials **2018**, 6, 1700791.

(144) Ling, H.; Yeo, L. P.; Wang, Z.; Li, X.; Mandler, D.; Magdassi, S.; Tok, A. I. Y. TiO

$_2$–WO$_3$ core–shell inverse opal structure with enhanced electrochromic performance in NIR region. Journal of Materials Chemistry C **2018**, 6, 8488–8494.

(145) Li, Y.; van de Groep, J.; Talin, A. A.; Brongersma, M. L. Dynamic Tuning of Gap Plasmon Resonances Using a Solid-State Electrochromic Device. Nano Letters **2019**, 19, 7988–7995.

(146) Rosseinsky, D. R.; Mortimer, R. J. Electrochromic Systems and the Prospects for Devices. Advanced Materials **2001**, 13, 783–793.

(147) Andrén, D.; Baranov, D. G.; Jones, S.; Volpe, G.; Verre, R.; Käll, M. Microscopic metavehicles powered and steered by embedded optical metasurfaces. Nature Nanotechnology **2021**, 16, 970–974.

(148) Badloe, T.; Lee, J.; Seong, J.; Rho, J. Tunable Metasurfaces: The Path to Fully Active Nanophotonics. Advanced Photonics Research 2000205.

(149) Guanxing, Z.; Liu, Z.; Deng, W.; Zhu, W. Reconfigurable metasurfaces with mechanical actuations: towards flexible and tunable photonic devices. Journal of Optics **2020**, 23, 013001.

(150) Chen, Y.; Ai, B.; Wong, Z. J. Soft optical metamaterials. Nano Convergence **2020**, 7, 1–17.

(151) Chang, Y.; Wei, J.; Lee, C. Metamaterials – from fundamentals and MEMS tuning mechanisms to applications. Nanophotonics **2020**, 9, 3049–3070.

(152) Algamili, A. S.; Khir, M. H. M.; Dennis, J. O.; Ahmed, A. Y.; Alabsi, S. S.; Hashwan, S. S. B.; Junaid, M. M. A review of actuation and sensing mechanisms in MEMS-based sensor devices. Nanoscale research letters **2021**, 16, 1–21.

(153) Meng, C.; Thrane, P. C.; Ding, F.; Gjessing, J.; Thomaschewski, M.; Wu, C.;

Dirdal, C.; Bozhevolnyi, S. I. Dynamic piezoelectric MEMS-based optical metasurfaces. Science Advances **2021**, 7.

(154) Bakke, T.; Vogl, A.; Żero, O.; Tyholdt, F.; Johansen, I.-R.; Wang, D. A novel ultra-planar, long-stroke and low-voltage piezoelectric micromirror. Journal of Micromechanics and Microengineering **2010**, 20, 064010.

(155) Ren, Z.; Chang, Y.; Ma, Y.; Shih, K.; Dong, B.; Lee, C. Leveraging of MEMS technologies for optical metamaterials applications. Advanced Optical Materials **2020**, 8, 1900653.

(156) Arbabi, E.; Arbabi, A.; Kamali, S. M.; Horie, Y.; Faraji-Dana, M.; Faraon, A. MEMS-tunable dielectric metasurface lens. Nature communications **2018**, 9, 1–9.

(157) Walia, S.; Shah, C. M.; Gutruf, P.; Nili, H.; Chowdhury, D. R.; Withayachumnankul, W.; Bhaskaran, M.; Sriram, S. Flexible metasurfaces and metamaterials: A review of materials and fabrication processes at micro- and nano-scales. Applied Physics Reviews **2015**, 2, 011303.

(158) Kamali, S. M.; Arbabi, A.; Arbabi, E.; Horie, Y.; Faraon, A. Decoupling optical function and geometrical form using conformal flexible dielectric metasurfaces. Nature communications **2016**, 7, 1–7.

(159) Xu, H.-X.; Hu, G.; Wang, Y.; Wang, C.; Wang, M.; Wang, S.; Huang, Y.; Genevet, P.; Huang, W.; Qiu, C.-W. Polarization-insensitive 3D conformal-skin metasurface cloak. Light: Science & Applications **2021**, 10, 1–13.

(160) Ee, H.-S.; Agarwal, R. Tunable metasurface and flat optical zoom lens on a stretchable substrate. Nano letters **2016**, 16, 2818–2823.

(161) Chen, S.; Liu, Z.; Du, H.; Tang, C.; Ji, C.-Y.; Quan, B.; Pan, R.; Yang, L.;

Li, X.; Gu, C., et al. Electromechanically reconfigurable optical nano-kirigami. Nature communications **2021**, <u>12</u>, 1–8.

(162) Wang, Z.; Jing, L.; Yao, K.; Yang, Y.; Zheng, B.; Soukoulis, C. M.; Chen, H.; Liu, Y. Origami-based reconfigurable metamaterials for tunable chirality. Advanced materials **2017**, <u>29</u>, 1700412.

(163) Han, Y.; Chen, S.; Ji, C.; Liu, X.; Wang, Y.; Liu, J.; Li, J. Reprogrammable optical metasurfaces by electromechanical reconfiguration. Optics Express **2021**, <u>29</u>, 30751.

(164) Kim, J.; Rana, A. S.; Kim, Y.; Kim, I.; Badloe, T.; Zubair, M.; Mehmood, M. Q.; Rho, J. Chiroptical Metasurfaces: Principles, Classification, and Applications. Sensors **2021**, <u>21</u>, Number: 13.

(165) Probst, P. T.; Mayer, M.; Gupta, V.; Steiner, A. M.; Zhou, Z.; Auernhammer, G. K.; König, T. A. F.; Fery, A. Mechano-tunable chiral metasurfaces via colloidal assembly. Nature Materials **2021**, <u>20</u>.

(166) On the Effect of Water-Induced Degradation of Thin-Film Piezoelectric Microelectromechanical Systems. <u>30</u>.

(167) Manjappa, M.; Pitchappa, P.; Singh, N.; Wang, N.; Zheludev, N. I.; Lee, C.; Singh, R. Reconfigurable MEMS Fano metasurfaces with multiple-input–output states for logic operations at terahertz frequencies. Nature Communications **2018**, <u>9</u>, 4056.

(168) de Gennes, P.; Prost, J. The Physics of Liquid Crystals; International Series of Monographs on Physics; 1993.

(169) Kawamoto, H. The history of liquid-crystal displays. Proceedings of the IEEE **2002**, <u>90</u>, 460–500.

(170) Otón, J. M.; Otón, E.; Quintana, X.; Geday, M. A. Liquid-crystal phase-only devices.

Journal of Molecular Liquids **2018**, 267, 469–483, Special Issue Dedicated to the Memory of Professor Y. Reznikov.

(171) Evans, P.; Wurtz, G.; Hendren, W.; Atkinson, R.; Dickson, W.; Zayats, A.; Pollard, R. Electrically switchable nonreciprocal transmission of plasmonic nanorods with liquid crystal. Applied Physics Letters **2007**, 91, 043101.

(172) Gorkunov, M. V.; Osipov, M. A. Tunability of wire-grid metamaterial immersed into nematic liquid crystal. Journal of Applied Physics **2008**, 103, 036101.

(173) Kim, Y.; Won, K.; An, J.; Hong, J.-Y.; Kim, Y.; Choi, C.-S.; Song, H.; Song, B.; Kim, H. S.; Bae, K.-D.; Burm, J.; Lee, H.-S. Large-area liquid crystal beam deflector with wide steering angle. Appl. Optics **2020**, 59, 7462–7468.

(174) Xie, Z.-W.; Yang, J.-H.; Vashistha, V.; Lee, W.; Chen, K.-P. Liquid-crystal tunable color filters based on aluminum metasurfaces. Optics Express **2017**, 25, 30764–30770.

(175) Sharma, M.; Ellenbogen, T. An All-Optically Controlled Liquid-Crystal Plasmonic Metasurface Platform. Laser & Photonics Reviews **2020**, 14, 2000253.

(176) Atorf, B.; Mühlenbernd, H.; Zentgraf, T.; Kitzerow, H. All-optical switching of a dye-doped liquid crystal plasmonic metasurface. Optics Express **2020**, 28, 8898–8908.

(177) Bosch, M.; Shcherbakov, M. R.; Won, K.; Lee, H.-S.; Kim, Y.; Shvets, G. Electrically Actuated Varifocal Lens Based on Liquid-Crystal-Embedded Dielectric Metasurfaces. Nano Letters **2021**, 21, 3849–3856.

(178) Li, S.-Q.; Xu, X.; Maruthiyodan Veetil, R.; Valuckas, V.; Paniagua-Domínguez, R.; Kuznetsov, A. I. Phase-only transmissive spatial light modulator based on tunable dielectric metasurface. Science **2019**, 364, 1087–1090.

(179) Li, J.; Yu, P.; Zhang, S.; Liu, N. Electrically-controlled digital metasurface device for light projection displays. Nature Communications **2020**, 11.

(180) Zhu, S.; Xu, Z.; Zhang, H.; Yang, K.; Wang, N.; Liu, H.; Wang, Y.; Xia, J.; Huang, L. Liquid crystal integrated metadevice for reconfigurable hologram displays and optical encryption. Optics Express **2021**, _29_, 9553–9564.

(181) Kim, I.; Kim, W.-S.; Kim, K.; Ansari, M. A.; Mehmood, M. Q.; Badloe, T.; Kim, Y.; Gwak, J.; Lee, H.; Kim, Y.-K.; Rho, J. Holographic metasurface gas sensors for instantaneous visual alarms. Science Advances **2021**, _7_.

(182) Liu, Y.; Song, J.; Zhao, W.; Ren, X.; Cheng, Q.; Luo, X.; Fang, N. X.; Hu, R. Dynamic thermal camouflage via a liquid-crystal-based radiative metasurface. Nanophotonics **2020**, _9_, 855–863.

(183) Wu, J.; Shen, Z.; Ge, S.; Chen, B.; Shen, Z.; Wang, T.; Zhang, C.; Hu, W.; Fan, K.; Padilla, W.; Lu, Y.; Jin, B.; Chen, J.; Wu, P. Liquid crystal programmable metasurface for terahertz beam steering. Applied Physics Letters **2020**, _116_, 131104.

(184) Shabanpour, J.; Sedaghat, M.; Nayyeri, V.; Oraizi, H.; Ramahi, O. M. Real-time multi-functional near-infrared wave manipulation with a 3-bit liquid crystal based coding metasurface. Optics Express **2021**, _29_, 14525–14535.

(185) Ting, T.-L. Technology of liquid crystal based antenna. Optics express **2019**, _27_, 17138–17153.

(186) Sun, M.; Xu, X.; Sun, X. W.; Liang, X.; Valuckas, V.; Zheng, Y.; Paniagua-Domínguez, R.; Kuznetsov, A. I. Efficient visible light modulation based on electrically tunable all dielectric metasurfaces embedded in thin-layer nematic liquid crystals. Scientific Reports **2019**, _9_.

(187) Su, H.; Wang, H.; Zhao, H.; Xue, T.; Zhang, J. Liquid-Crystal-Based Electrically Tuned Electromagnetically Induced Transparency Metasurface Switch. Scientific Reports **2017**, _7_.

(188) Lininger, A.; Zhu, A. Y.; Park, J.-S.; Palermo, G.; Chatterjee, S.; Boyd, J.; Capasso, F.; Strangi, G. Optical properties of metasurfaces infiltrated with liquid crystals. Proceedings of the National Academy of Sciences **2020**, 117, 20390–20396.

(189) Dolan, J. A.; Cai, H.; Delalande, L.; Li, X.; Martinson, A. B. F.; de Pablo, J. J.; López, D.; Nealey, P. F. Broadband Liquid Crystal Tunable Metasurfaces in the Visible: Liquid Crystal Inhomogeneities Across the Metasurface Parameter Space. ACS Photonics **2021**, 8, 567–575.

(190) Xu, J.; Yang, R.; Fan, Y.; Fu, Q.; Zhang, F. A Review of Tunable Electromagnetic Metamaterials With Anisotropic Liquid Crystals. Frontiers in Physics **2021**, 9, 67.

(191) Buchnev, O.; Podoliak, N.; Kaczmarek, M.; Zheludev, N. I.; Fedotov, V. A. Electrically Controlled Nanostructured Metasurface Loaded with Liquid Crystal: Toward Multifunctional Photonic Switch. Advanced Optical Materials **2015**, 3, 674–679.

(192) Gorkunov, M. V.; Kasyanova, I. V.; Artemov, V. V.; Barnik, M. I.; Geivandov, A. R.; Palto, S. P. Fast Surface-Plasmon-Mediated Electro-Optics of a Liquid Crystal on a Metal Grating. Phys. Rev. Applied **2017**, 8, 054051.

(193) Franklin, D.; Chen, Y.; Vázquez-Guardado, A.; Modak, S.; Boroumand, J.; Xu, D.; Wu, S.-T.; Chanda, D. Polarization-independent actively tunable colour generation on imprinted plasmonic surfaces. Nature Communications **2015**, 6.

(194) Kowerdziej, R.; Wróbel, J.; Kula, P. Ultrafast electrical switching of nanostructured metadevice with dual-frequency liquid crystal. Scientific reports 9, 1–8.

(195) Akselrod, G. M.; Yang, Y.; Bowen, P. Tunable liquid crystal metasurfaces. U.S. Patent 20200303826 A1, September 24 2020.

(196) Ma, Y.; Tam, A. M. W.; Gan, X. T.; Shi, L. Y.; Srivastava, A. K.; Chigrinov, V. G.;

Kwok, H. S.; Zhao, J. L. Fast switching ferroelectric liquid crystal Pancharatnam-Berry lens. Optics Express **2019**, 27, 10079–10086.

(197) Tsilipakos, O. et al. Toward Intelligent Metasurfaces: The Progress from Globally Tunable Metasurfaces to Software-Defined Metasurfaces with an Embedded Network of Controllers. Advanced Optical Materials **2020**, 8, 2000783.

(198) Zhang, W.; Mazzarello, R.; Wuttig, M.; Ma, E. Designing crystallization in phase-change materials for universal memory and neuro-inspired computing. Nature Reviews Materials **2019**, 4.

(199) Wu, C.; Yu, H.; Lee, S.; Peng, R.; Takeuchi, I.; Li, M. Programmable phase-change metasurfaces on waveguides for multimode photonic convolutional neural network. Nature Communications **2021**, 12, 96.

(200) Kwon, H.; Zheng, T.; Faraon, A. Nano-electromechanical Tuning of Dual-Mode Resonant Dielectric Metasurfaces for Dynamic Amplitude and Phase Modulation. Nano Letters **2021**, 21, 2817–2823.

(201) Shaltout, A.; Kildishev, A.; Shalaev, V. Time-varying metasurfaces and Lorentz non-reciprocity. Optical Materials Express **2015**, 5, 2459–2467.

(202) Achouri, K.; Caloz, C. Electromagnetic Metasurfaces Theory and Applications; 2021.

(203) Caloz, C.; Alù, A.; Tretyakov, S.; Sounas, D.; Achouri, K.; Deck-Léger, Z.-L. What is Nonreciprocity? Physical Review Applied **2018**, 10, 047001, arXiv: 1804.00235.

(204) Asadchy, V. S.; Mirmoosa, M. S.; Díaz-Rubio, A.; Fan, S.; Tretyakov, S. A. Tutorial on Electromagnetic Nonreciprocity and its Origins. Proceedings of the IEEE **2020**, 108, 1684–1727.

(205) Caloz, C.; Alu, A.; Tretyakov, S.; Sounas, D.; Achouri, K.; Deck-Léger, Z.-L. Electromagnetic nonreciprocity. Physical Review Applied **2018**, 10, 047001.

(206) Caloz, C.; Deck-Léger, Z.-L. Spacetime metamaterials—part I: general concepts. IEEE Transactions on Antennas and Propagation **2019**, 68, 1569–1582.

(207) Caloz, C.; Deck-Léger, Z.-L. Spacetime metamaterials—part II: theory and applications. IEEE Transactions on Antennas and Propagation **2019**, 68, 1583–1598.

(208) Maznev, A.; Every, A.; Wright, O. Reciprocity in reflection and transmission: What is a 'phonon diode'? Wave Motion **2013**, 50, 776–784.

(209) Krasnok, A.; Tymchenko, M.; Alù, A. Nonlinear metasurfaces: a paradigm shift in nonlinear optics. Materials Today **2018**, 21, 8–21.

(210) Hadad, Y.; Sounas, D. L.; Alu, A. Space-time gradient metasurfaces. Physical Review B **2015**, 92, 100304.

(211) Taravati, S.; Eleftheriades, G. V. Full-duplex nonreciprocal beam steering by time-modulated phase-gradient metasurfaces. Physical Review Applied **2020**, 14, 014027.

(212) Guo, X.; Ding, Y.; Duan, Y.; Ni, X. Nonreciprocal metasurface with space–time phase modulation. Light: Science & Applications **2019**, 8, 1–9.

(213) Zhang, L.; Chen, X. Q.; Liu, S.; Zhang, Q.; Zhao, J.; Dai, J. Y.; Bai, G. D.; Wan, X.; Cheng, Q.; Castaldi, G., et al. Space-time-coding digital metasurfaces. Nature communications **2018**, 9, 1–11.

(214) Zhang, L.; Chen, X. Q.; Shao, R. W.; Dai, J. Y.; Cheng, Q.; Castaldi, G.; Galdi, V.; Cui, T. J. Breaking Reciprocity with Space-Time-Coding Digital Metasurfaces. Advanced Materials **2019**, 31, 1904069.

(215) Liu, M.; Powell, D. A.; Zarate, Y.; Shadrivov, I. V. Huygens' Metadevices for Parametric Waves. Phys. Rev. X **2018**, 8, 031077.

(216) Liu, B.; Wong, S.-W.; Li, Y. Rotational Doppler effect by space-time-coding meta-surfaces for nonreciprocal electromagnetic isolation. Optics Express **2021**, 29, 24500–24507.

(217) Taravati, S.; Eleftheriades, G. V. Four-dimensional wave transformations by space-time metasurfaces. arXiv preprint arXiv:2011.08423 **2020**,

(218) Shi, Y.; Fan, S. Dynamic non-reciprocal meta-surfaces with arbitrary phase reconfig-urability based on photonic transition in meta-atoms. Applied Physics Letters **2016**, 108, 021110.

(219) Wang, X.; Caloz, C. Advances in Spacetime-Modulated Metasurfaces. 2020 XXXII-Ird General Assembly and Scientific Symposium of the International Union of Radio Science. 2020; pp 1–3.

(220) Asadchy, V. S.; Díaz-Rubio, A.; Tretyakov, S. A. Bianisotropic metasurfaces: physics and applications. Nanophotonics **2018**, 7, 1069–1094.

(221) Caloz, C.; Sihvola, A. Electromagnetic Chirality, Part 1: The Microscopic Perspective [Electromagnetic Perspectives]. IEEE Antennas and Propagation Magazine **2020**, 62, 58–71, Conference Name: IEEE Antennas and Propagation Magazine.

(222) Pfeiffer, C.; Zhang, C.; Ray, V.; Guo, L. J.; Grbic, A. High Performance Bianisotropic Metasurfaces: Asymmetric Transmission of Light. Phys. Rev. Lett. **2014**, 113, 023902.

(223) Ra'di, Y.; Grbic, A. Magnet-free nonreciprocal bianisotropic metasurfaces. Phys. Rev. B **2016**, 94, 195432.

(224) Ramaccia, D.; Sounas, D. L.; Alù, A.; Toscano, A.; Bilotti, F. Phase-induced frequency conversion and doppler effect with time-modulated metasurfaces. IEEE Transactions on Antennas and Propagation **2019**, 68, 1607–1617.

(225) Ra'di, Y.; Alù, A. Nonreciprocal Wavefront Manipulation in Synthetically Moving Metagratings. Photonics 2020, 7.

(226) Wang, X.; Ptitcyn, G.; Asadchy, V. S.; Díaz-Rubio, A.; Mirmoosa, M. S.; Fan, S.; Tretyakov, S. A. Nonreciprocity in Bianisotropic Systems with Uniform Time Modulation. Phys. Rev. Lett. 2020, 125, 266102.